

# We are IntechOpen, the world's leading publisher of Open Access books Built by scientists, for scientists

6,900

Open access books available

185,000

International authors and editors

200M

Downloads

Our authors are among the

154

Countries delivered to

TOP 1%

most cited scientists

12.2%

Contributors from top 500 universities



WEB OF SCIENCE™

Selection of our books indexed in the Book Citation Index  
in Web of Science™ Core Collection (BKCI)

Interested in publishing with us?  
Contact [book.department@intechopen.com](mailto:book.department@intechopen.com)

Numbers displayed above are based on latest data collected.  
For more information visit [www.intechopen.com](http://www.intechopen.com)



# Imaging of Radiation Accidents and Radioactive Contamination Using Scintillators

Tomoya Ogawa et al.\*

*Laboratory of Crystal Physics and Technology  
Japan*

## 1. Introduction

An accident in a nuclear power plant, which can be caused by an unpredictable event such as an explosion, fire, and earthquake, has severe and far-reaching consequences. Therefore, it is crucial to carefully and constantly monitor the plant and precisely detect any radiation source. Radiation contamination in laboratories and in the environment due to nuclear fallout is among the issues that require an immediate solution. Radiation detection has become increasingly important because of the increasing number of nuclear power plants that have been established to replace conventional power plants, as part of the effort to suppress carbon dioxide emission. For these purposes, this chapter will discuss the principle and method of mapping flying radiations. Visual mapping of intensity and direction of

---

\* Nobuhiko Sarukura<sup>2</sup>, Masahito Watanabe<sup>3</sup>, Tsuguo Fukuda<sup>4</sup>, Nobuhito Nango<sup>5</sup>, Yasunobu Arikawa<sup>2</sup>, Kohei Yamanoi<sup>2</sup>, Tomoharu Nakazato<sup>2</sup>, Marilou Cadatal-Raduban<sup>2</sup>, Toshihiko Shimizu<sup>2</sup>, Mitsuo Nakai<sup>2</sup>, Takayoshi Norimatsu<sup>2</sup>, Hiroshi Azechi<sup>2</sup>, Takahiro Murata<sup>6</sup>, Shigeru Fujino<sup>7</sup>, Hideki Yoshida<sup>8</sup>, Kei Kamada<sup>9</sup>, Yoshiyuki Usuki<sup>9</sup>, Toshihisa Suyama<sup>10</sup>, Akira Yoshikawa<sup>11</sup>, Nakahiro Sato<sup>12</sup>, Hirofumi Kan<sup>12</sup>, Hiroaki Nishimura<sup>2</sup>, Kunioki Mima<sup>2</sup>, Masahito Hosaka<sup>13</sup>, Masahiro Katoh<sup>14</sup>, Nobuhiro Kosugi<sup>14</sup>, Kentaro Fukuda<sup>10</sup>, Takayuki Yanagida<sup>11</sup>, Yuui Yokota<sup>11</sup>, Fumio Saito<sup>11</sup>, Kouhei Sakai<sup>2</sup>, Dirk Ehrentauf<sup>11</sup>, Mitsuru Nagasono<sup>15</sup>, Tadashi Togashi<sup>15</sup>, Atsushi Higashiya<sup>15</sup>, Makina Yabashi<sup>15</sup>, Tetsuya Ishikawa<sup>15</sup>, Haruhiko Ohashi<sup>15,16</sup>, and Hiroaki Kimura<sup>15,16</sup>

<sup>2</sup>*Institute of Laser Engineering, Osaka University, Japan*

<sup>3</sup>*Department of Physics, Gakushuin University, Japan*

<sup>4</sup>*Fukuda Crystal Laboratory, Japan*

<sup>5</sup>*Ratoc System Engineering Co., Japan*

<sup>6</sup>*Department of Chemistry, School of Science, Tokai University, Japan*

<sup>7</sup>*Department of Materials Process Engineering, Graduate School of Engineering, Kyushu University, Japan*

<sup>8</sup>*Ceramic Research Center of Nagasaki, Japan*

<sup>9</sup>*Furukawa Co., Ltd., Japan*

<sup>10</sup>*Tokuyama Corporation, Japan*

<sup>11</sup>*Institute of Multidisciplinary Research for Advanced Materials, Tohoku University, Japan*

<sup>12</sup>*Central Research Laboratory, Hamamatsu Photonics K.K., Japan*

<sup>13</sup>*Graduate School of Engineering, Nagoya University, Japan*

<sup>14</sup>*UVSOR Facility Institute for Molecular Science, Japan*

<sup>15</sup>*RIKEN XFEL Project Head Office, Japan*

<sup>16</sup>*Japan Synchrotron Radiation Research Institute, Japan*

incident radiations is necessary to detect any radiation accident and/or invisible radiation contamination. Discussion will focus on directional detection of radiation sources, being the minimum requirement for identifying and characterizing unpredictable accidents and contamination.

Specifically, this chapter will discuss two-dimensional imaging of radiation accidents and radioactive contamination. It will also detail the development of a “panchromatic” detector that is suitable for use against radiation from different types of sources. This detector combines several types of scintillating elements into a bundle, which is composed of well-designed and regularly arranged scintillation fiber-segments or thin cylinders to detect and display the radiation sources as a map, using the directional sensitivity of the segments or cylinders for locating sources of incident radiation. In addition, this chapter will discuss the numerical designs and the characteristics of two detector configurations. These are the telescope configuration, wherein all the extended lines of the scintillator fiber segments or thin cylinders composing the bundle are focused to a point; and the magnifier configuration, wherein all the extended lines of the segments within the bundle are diverging from the focus.

An integral part of the radiation detector is the scintillator. Scintillators are created and developed to correctly detect and count incident radiations. In this regard, part of this chapter will also be devoted to the discussion of the properties of scintillators that are ideal for use in radiation detectors. In particular, the effect of scintillator shape and decay time will be outlined, leading to the attributes of an ideal imaging scintillator. For instance, one of the size effects is the directional sensitivity to incident radiations. This can be realized by using a thin cylinder-type or a fiber segment-type scintillator. The output signals from the thin cylinder are proportional to the number of radiations that passed through it, if its length is good enough to absorb the incident radiations.

To complete the chapter, the performance of various scintillators will be discussed. Among the scintillators that will be discussed is the praseodymium-doped lithium glass (APLF80+3Pr), cerium-doped lutetium lithium fluoride ( $\text{Ce}^{3+}:\text{LuLiF}_4$ ), zinc oxide (ZnO), and neodymium-doped lanthanum fluoride ( $\text{Nd}^{3+}:\text{LaF}_3$ ).

## 2. Scintillators

Scintillators are fluorescent materials that mediate the detection of high energy (ionizing) electromagnetic or charged particle radiation. A scintillator absorbing high-energy radiation fluoresces at a characteristic Stokes-shifted (longer) wavelength that can be detected by conventional detectors like photodiodes or photomultiplier tubes. If the properties of the scintillator are known, then the high-energy radiation that it absorbed can in turn be characterized. Radiation detectors are typically useful for imaging by utilizing high-penetration power radiation and for spectroscopy by utilizing characteristic radiation from each atom. As part of a detection unit, the broad application of scintillators comprises various scientific disciplines such as high-energy physics, nuclear physics, astronomy, and mineral exploration. It has also found applications in product quality control, airport security, nuclear safeguards verification, cargo container inspection, toxic dumpsite monitor, and environmental monitoring. Moreover, Positron Emission Tomography (PET) for medical imaging has gained popularity as a common clinical tool for detection of tumors.

### 2.1 Shape of scintillators

Scintillation is caused by collision between a high-energy radiation and an electron belonging to a heavy dopant atom. This collision is considered as one of the ideal stochastic processes. As such, a scintillation detector is usually prepared as a very large block to correctly count incident radiations while excluding its size effects.

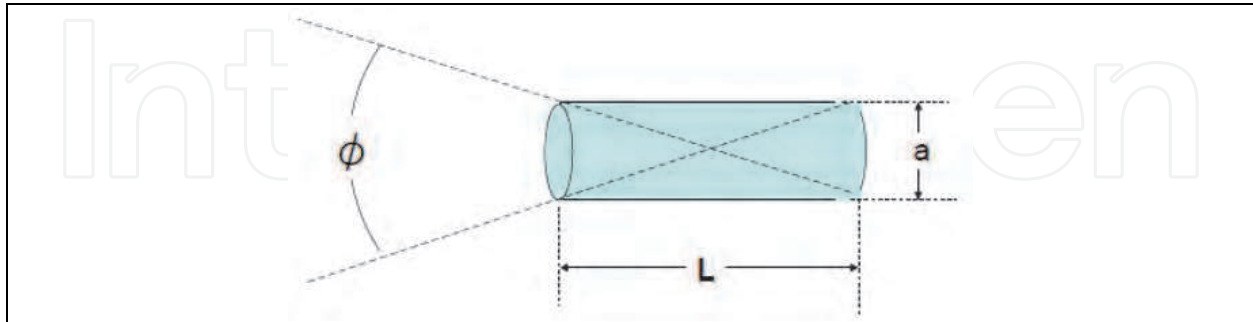


Fig. 1. A thin cylinder or fiber segment scintillator and its incident radiation acceptance angle, where  $a$  is its diameter,  $L$  is its length, and  $\Phi$  is the divergence of its sensitivity against incoming radiation.

One of the size effects is the directional sensitivity to incident radiations. This can be realized by using a thin cylinder-type or a fiber segment-type scintillator. The output signals from the thin cylinder are proportional to the number of radiations that passed through it if its length is good enough to absorb the incident radiations. On the other hand, radiations crossing obliquely through a segment may or may not generate scintillation even if every radiation were moving along an identical line. This can, therefore, constitute random noise. The signals arising from radiation passing directly through the scintillator can be separated from the random noise generated by radiation crossing the scintillator obliquely through the well-known noise reduction technique using multi-integration.

In most materials, the refractive index for high energy radiations is nearly equal to unity. Therefore, the aperture,  $\Phi$ , of the cylinder for which incident radiations is detected is

$$2\tan^{-1}(a/L) \quad (1)$$

where  $L$  and  $a$  are the cylinder length and diameter, respectively, as illustrated in Fig. 1. Surface smoothness of the cylinder is very important since multiple scattering of the scintillation light at its surface is detrimental to the imaging of output light signals.

### 2.2 The decay time of scintillation

Since scintillators are created and developed to correctly detect and count incident radiations, a very short scintillation decay time is desirable for precise time-resolved radiation measurement. Decay time of well-known scintillators is much less than one microsecond. For the case of scintillators developed mainly for imaging, measurement is limited by the refresh rate of the television or monitor. The refresh rate of monitors and televisions is typically 30 frames per second. It is therefore acceptable that the decay time of imaging scintillators is in the millisecond range. This decay time is longer than the requirement for scintillators used in radiation counting. For this purpose, development of brighter scintillators without regard to decay times would be of primary importance when developing an imaging device.

### 2.3 Scintillation crystals

A comparison of the performance of different scintillator materials is shown in Table 1 (Ishii & Kobayashi, 1991, 2007). One of the best candidates for imaging will be thin scintillation cylinders made from CsI:Tl crystals. This material is ideal as an imaging scintillator because among the materials in Table 1, it has the largest photoluminescence output per radiation energy of 59,000 photons/MeV. It also has a relatively long decay time of 1  $\mu$ s. Moreover, it has a high melting point of 621°C and is only slightly hygroscopic.

Material	Density (g/cm <sup>3</sup> )	Radiation length, X <sub>0</sub> (cm)	PL output (Photons/MeV)	Decay (ns)	Application
NaI:Tl	3.67	2.59	38000	230	General purpose
CsF	4.11	2.23	2000	2.8	
CsI:Tl <sup>+</sup>	4.53	1.86	59000	1050	X-CT
CsI	4.51	1.85	30*	6, 35	
Bi <sub>4</sub> Ge <sub>3</sub> O <sub>12</sub>	7.13	1.12	8200	300	PCT, NP, HE
CdWO <sub>4</sub>	7.68	1.06	15000	5000	X-CT
Gd <sub>2</sub> SiO <sub>5</sub> :Ce	6.71	1.38	10000	60	PET
Lu <sub>2</sub> SiO <sub>5</sub> :Ce	7.4	1.14	30000	40	PET
PbWO <sub>4</sub>	8.2	0.92	490	10	HE

NP: Nuclear physics experiment

\* Faster decay component

HE: High energy physics experiment

+ Slight hygroscopicity

Table 1. Characteristic features of scintillation crystals

### 3. Configuration and compilation of the scintillation thin cylinders

Visual mapping of intensity and direction of incident radiations is necessary to detect any radiation accident and/or invisible radiation contamination. For this purpose, thin cylinder scintillators or fiber segments are compiled to form a bundle where every extended line of the cylinder is either focused into a point, as shown in Fig. 2 or diverging from a point, as shown in Fig. 3. The former is referred to as the telescope configuration while the latter is referred to as the magnifier configuration (Ogawa, 2007, 2010).

#### 3.1 Telescope configuration

Figure 2 demonstrates a typical telescope configuration. The terminal end of the scintillation cylinder bundle where the focus side is located is optically connected to a two dimensional photodetector, such as a charge coupled device (CCD). An image intensifier or a micro-imaging plate is used to amplify the signals before reaching the CCD.

The field angle or aperture of this telescope is determined by  $R$  and  $F$ , where  $R$  is the diameter of the circle circumscribed by the terminal ends and  $F$  is the distance between the focus and the terminal plane. With this configuration, the intensity and direction of incident radiations will be indicated as a map on the computer, after image processing.

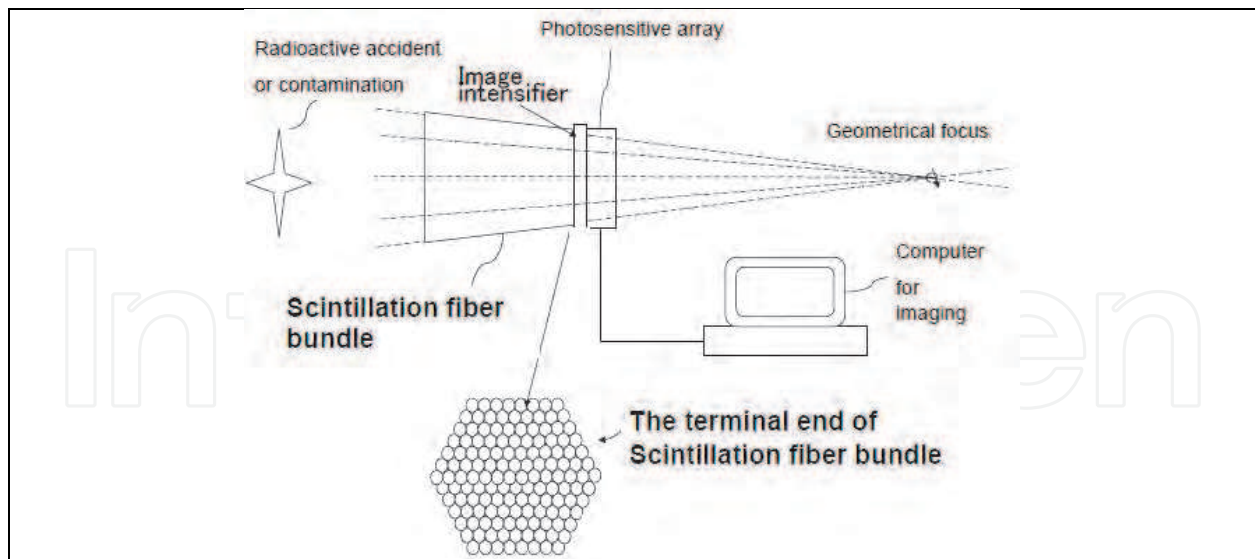


Fig. 2. The telescopic configuration. All the extended lines of the scintillator fiber segments or thin cylinders composing the bundle are focused to a point.

### 3.2 Magnifier configuration

For the magnifier configuration, the size of the focal point is nearly equal to or a little larger than the diameter of the fiber. In this configuration, a radiation source such as an X-ray tube or a small block of  $^{60}\text{Co}$  is continuously emitting its radiation at the focal point. On the other hand, the specimen being studied is placed at a plane between the focus and the front of the bundle. This way, the transparency of this specimen against the radiation will be observed as its magnified image. This is similar to an optical magnifier. If radiation substances or radioactive isotopes are scattered on a plane, a map of this contamination will be observed when the focus of the magnifier either approaches or departs from that plane, as shown in Fig. 3.

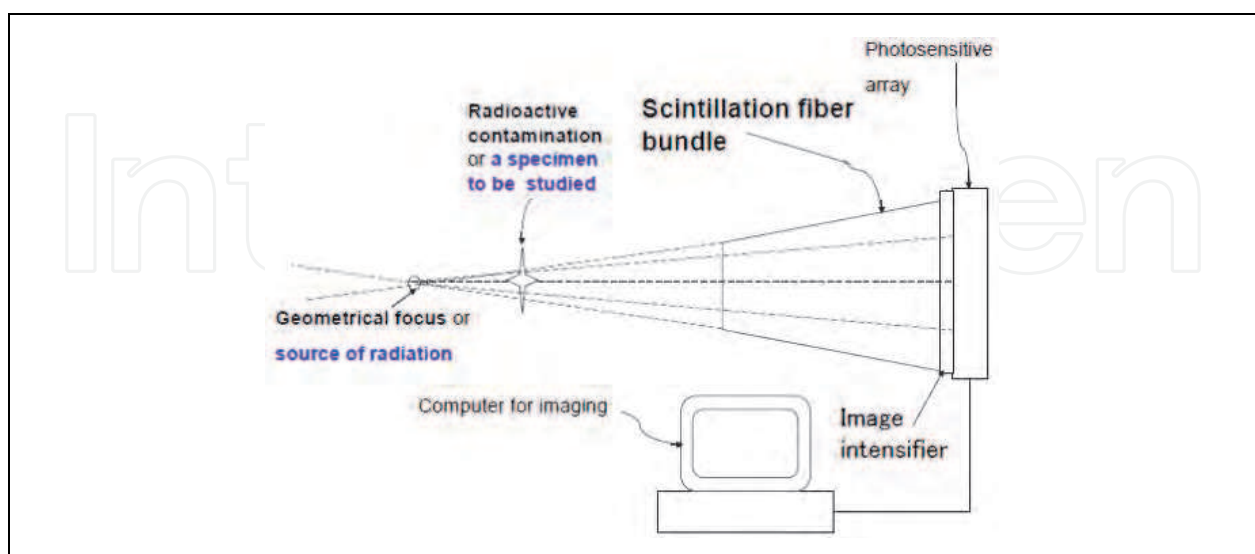


Fig. 3. The magnifier configuration. All the extended lines of the segments within the bundle are diverging from the focus.

## 4. Numerical designs

In this section, we discuss the numerical considerations for designing the telescope and magnifier configurations. In particular, the characteristic features of the cylinders to be used in the telescope configuration as well as the diameter of the fiber segments for the magnifier configuration are discussed.

### 4.1 Numerical designs of cylinders for the telescope configuration

The sensitivity divergence,  $\Phi$ , of a thin scintillation cylinder and the aperture for imaging,  $\Theta$ , of the cylinder bundle are defined as follows:

$$\Phi = 2 \tan^{-1}(a/L) \quad (2)$$

$$\Theta = 2 \tan^{-1}(R/F) \quad (3)$$

On the other hand, the total number of the cylinders,  $N$ , is given by

$$N = 3n(n+1) + 1 \quad (4)$$

where  $n$  is number of cylinders along the radius of the circle circumscribed by the terminal ends. Thus  $\Theta$ ,  $\Phi$  and  $n$  are related as follows:

$$\Phi = (\Theta/2n)p \quad (5)$$

In this equation,  $p$  is an overlapping or tolerance factor of the scintillation cylinder or fiber segment. In our calculations, we chose  $\Theta$  as  $47^\circ$ ,  $24^\circ$ ,  $8^\circ$ , and  $2.5^\circ$  because these apertures correspond to the 50 mm, 100 mm, 300 mm and 1000 mm focal length lens of the 35 mm camera system, respectively.

The length of a cylinder,  $L$ , is such that the incident radiation is enough to be absorbed for scintillation but the light generated within it will be perfectly received at the terminal end. In our calculations,  $L$  was assumed to be

$$L = 5X_0 \quad (6)$$

where  $X_0$  is the radiation length of the scintillation material. In this case, the incident radiation will be attenuated to  $1/e$ , which is equal to 0.0067 times (Fukuda et al., 2004). This attenuation value is acceptable for the present purpose. The radiation length of various scintillators is summarized in Table 1. As an example, by using a CsI:Tl crystal having an  $X_0$  of 18.6 mm, the suitable crystal length,  $L$ , would be 93 mm. Correspondingly, the diameter,  $a$ , of the CsI:Tl cylinders can be obtained using equations (2) and (5) with  $p = 2$ . Calculation results of the diameter of CsI:Tl cylinders for different apertures ( $\Theta$ ) and number of cylinders ( $n$ ) are shown in Table 2. It is worth mentioning that the diameter of the commercially available  $\text{Bi}_4\text{Ge}_3\text{O}_{12}$  (BGO) cylinders is 0.6 times compared to that of CsI:Tl because the radiation length of BGO is 0.60 times shorter than that of CsI:Tl.

### 4.2 Numerical designs of fiber segments for the magnifier configuration

The size of the focal point is nearly equal to or a little larger than the diameter of the fiber segment, as indicated in Fig.3. It is, therefore, more desirable to make thinner fiber segments. Today, the diameter of commercially available scintillation fibers, for example the BGO fiber is about  $30 \mu\text{m}$  (Fukuda & Chani, 2007; Fukuda et al., 2004). This is very similar in size to the focus of a commercial microfocus X-ray tube. If fibers with a  $1 \mu\text{m}$  diameter were

available, the resolution of the transparent image against radiation will clearly be improved because the half shadow of the image will be dramatically diminished.

(The case when  $p = 2$ )

$\theta$ \ n N	10	20	50	100
	331	1261	7651	30.301
47° (f = 50)	3.82 mm	1907 $\mu\text{m}$	763 $\mu\text{m}$	381 $\mu\text{m}$
24° (f = 100)	1.95 mm	970 $\mu\text{m}$	380 $\mu\text{m}$	195 $\mu\text{m}$
8° (f = 300)	0.65 mm	325 $\mu\text{m}$	130 $\mu\text{m}$	65 $\mu\text{m}$
2.5° (f = 1000)	0.20 mm	101 $\mu\text{m}$	41 $\mu\text{m}$	20 $\mu\text{m}$

The value of  $f$  in the parentheses indicates focal length of the lens with the same aperture under the film size: 35-mm camera system.

Table 2. The diameter of CsI:Tl scintillation cylinders

## 5. Scintillators for time-resolved measurement

As mentioned in Section 2.2, a very short scintillation decay time is desirable for precise time-resolved radiation measurement. Over the past years, several scintillators have been studied for this purpose, wherein several schemes have been considered in order to improve the response time of fluoride, oxide, and glass scintillators. In this section, the characteristics of fluoride, oxide, and glass scintillators will be discussed. Emphasis will be given to the improvement in the fluorescence decay time. In particular, the scintillation properties of cerium-doped lutetium lithium fluoride ( $\text{Ce}^{3+}:\text{LuLiF}_4$ ), praseodymium-doped lithium glass (APLF80 + 3Pr), neodymium-doped lanthanum fluoride ( $\text{Nd}^{3+}:\text{LaF}_3$ ), and zinc oxide (ZnO) will be discussed.

### 5.1 Pr-doped glass

In the field of fusion research, understanding the plasma dynamics could very well be the key in feasibly attaining controlled fusion. Moreover, studying the scattered neutrons is currently the most viable way of probing the fusion plasma. For this reason, neutron diagnostics is an indispensable tool for both inertial confinement fusion (ICF) and magnetic confinement fusion research (Cheon et al., 2008; Glebov et al., 2006; K.A. Tanaka et al., 2004; Lerche et al., 1995; Petrizzi et al., 2007; Ress et al., 1988). In particular, the observation of scattered neutrons from the high-density imploded deuterium plasma in laser fusion experiments is desired (Izumi et al., 2003). At the center of the imploded deuterium fuel plasma, deuterium-deuterium (DD) neutrons having energy of 2.45 MeV and scattered neutrons from the fuel deuteron are generated. The scattering probability depends only on the plasma areal density, which is the radial integral of density  $\rho R$ , in units of  $\text{g}/\text{cm}^2$ . In addition, a wide observable range of up to 3  $\text{g}/\text{cm}^2$  is required for future fusion reactors. These factors make the scattered neutron diagnostics method, highly expected to be further developed as an invaluable tool in ICF research. For this purpose, a fast-response neutron scintillator with a high cross section for scattered neutrons is strongly required.

The nuclear reaction,



has a large cross section resonant peak, well-fit to the back scattered neutron spectrum peak around 0.27 MeV, and a large Q value producing enough photons for lower energy scattered neutrons. Thus, a  ${}^6\text{Li}$  scintillator with a high lithium density is an ideal detector for this method (Izumi et al., 2003). Since scattered neutrons having energy around 0.27 MeV must be discriminated from the overwhelming majority of the 2.45 MeV primary neutrons or x-rays via time-of-flight experiments, a sufficiently fast time response is required. Moreover we must also discriminate the neutrons scattered by the experimental setup itself such as the vacuum chamber wall. Thus, the detector has to be placed at close proximity to the fusion plasma; necessitating a scintillator with a time decay of less than 20 ns. In this work, results are presented on the fast response time of a custom-developed  $\text{Pr}^{3+}$  (Praseodymium)-doped lithium glass as a scintillator material (Arikawa et al., 2009).

The  $\text{Pr}^{3+}$  ion with a higher emission cross section in the deep ultraviolet region (~270 nm) is preferred as a dopant (Yoshikawa et al., 2008) over the slower, albeit more widely-used  $\text{Ce}^{3+}$  (Cerium) ion with its smaller emission cross section at longer wavelengths (Ehrlich et al., 1979; Fairley & Spowart, 1978; Suzuki et al., 2002). Additionally, high Li-density fluoro-lithium glass is chosen as the host material over UV-transparent, Li-doped fluoride crystals such as  $\text{LiCaAlF}_6$ , primarily due to its ease-of-preparation and design flexibility.

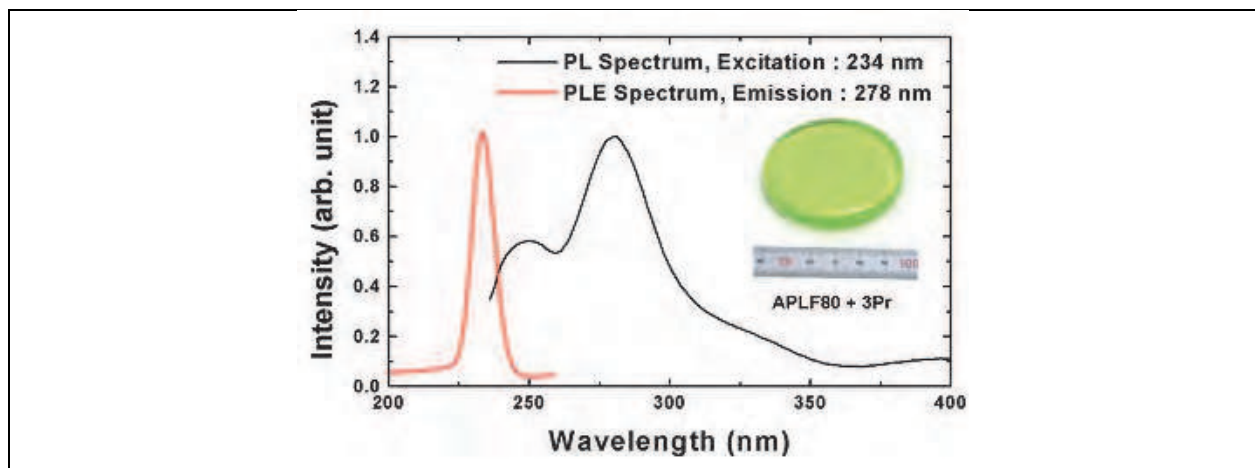


Fig. 4. Photoluminescence (PL) and photoluminescence excitation (PLE) spectrum of the APLF80+3Pr. The PL peak is observed at 279 nm while the PLE maximum occurs at 234 nm. The photograph shows the glass scintillator sample. The diameter is 6cm with a thickness of 1 cm.

The APLF80 + 3Pr glass sample, having a composition of  $20\text{Al}(\text{PO}_3)_3 - 80\text{LiF} + 3\text{PrF}_3$  (in mol) using 95.5%  ${}^6\text{Li}$  enriched lithium fluoride, is shown in the inset of Fig. 4. It was prepared using the melt-quenching method, where  $\text{PrF}_3$ -containing starting materials were melted in a glassy carbon crucible at 1100 degrees Celsius under nitrogen atmosphere. The glass melt was then cooled down to 400 degrees Celsius in the furnace, and subsequently annealed near the glass transition temperature. The lithium density was measured using an atomic absorption photometer to be 7.98 w%, 31.6 mmol/cc. This is the highest reported value for conventional  ${}^6\text{Li}$  glass scintillators, thus far (Saint-Gobain Crystals, 2007-2008). Fluorescence increase upon  ${}^{241}\text{Am}$ -alpha excitation was observed with higher doping of  $\text{Pr}^{3+}$ . The highest doping of  $\text{Pr}^{3+}$  was found to be 3% at the present manufacturing procedure. The preliminary characteristics were reported in (Murata et al., 2009).

Before the neutron observation experiments were conducted, the spectral- and temporal-optical characteristics of the sample were evaluated. From the peak of the pulse height distribution of the APLF80+3Pr sample, we estimated the fluorescence photons yield to be about 300 photons / 5.5 MeV-alpha, taking into consideration the limited acceptance angle of the photomultiplier window even though the emission can be regarded to be isotropic in all directions. Figure 4 shows the photoluminescence (PL) and photoluminescence excitation (PLE) spectra of the sample. Strong emission at around 278 nm due to the 5d-4f transition, which was the design wavelength, was seen. Furthermore, the host material was found to have good transmission in the vacuum ultraviolet region down to 180 nm, and no absorption at the luminescence region was observed.

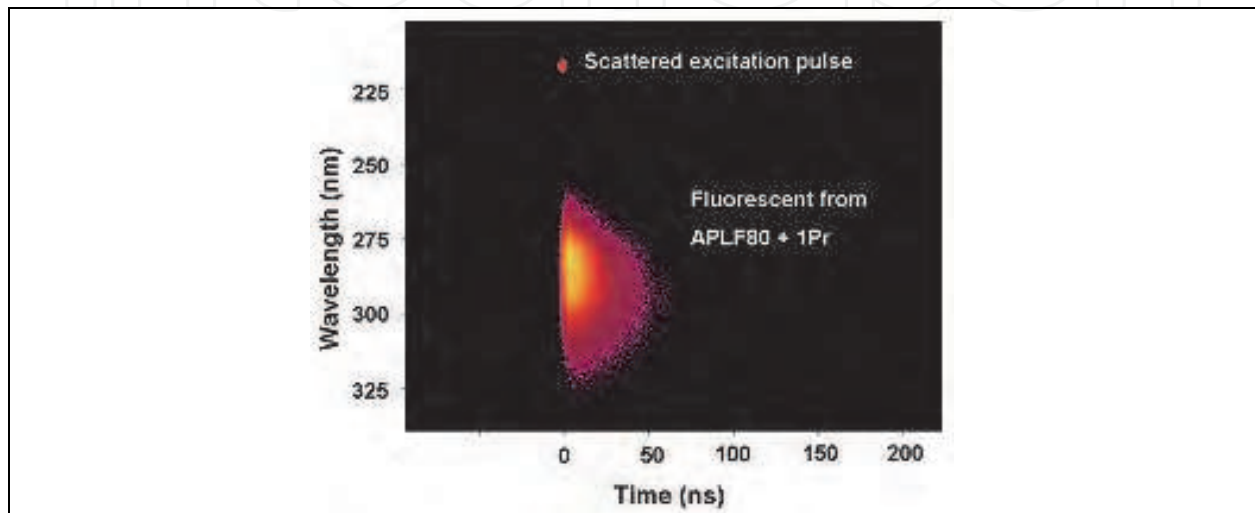


Fig. 5. Streak camera image of the spectral and time resolved luminescence of the APLF+1Pr. The excitation source is the 4th harmonics of a Ti: Sapphire laser.

The spectrally-resolved fluorescence lifetime of the APLF80+1Pr sample, excited with 217-nm 150, fs pulses using the 4th harmonics of a Ti:sapphire laser, was measured using a streak camera as shown in Fig. 5. The spectrally-integrated fluorescence decay profile, along with the other decay profiles for other excitation sources are shown in Fig. 6; where all the decay curves were fitted with a single exponential decay in the region from 50 % to 10 % of the peak value. For ultraviolet excitation, the fluorescence lifetime was determined to be  $19.5 \pm 0.80$  ns. The decay from short x-ray excitation pulses from laser-produced plasma was measured to be  $20.8 \pm 0.85$  ns. In this experiment, a 10- $\mu$ m thick aluminum plate target was irradiated by 4 ps/80 J Nd-glass laser pulses. The generated electron energy spectrum of a few MeV at the peak was also measured using an electron spectrometer. On the other hand, the fluorescence decay profile for 5.5 MeV  $^{241}\text{Am}$  alpha-particle excitation was  $6.7 \pm 0.03$  ns. Neutron excitation, having energy from 0.5 MeV to 10 MeV using  $^{252}\text{Cf}$ , exhibited the fastest decay time of  $5.9 \pm 0.16$  ns. This significant difference of decay times for neutrons and x-ray excitation is preferable for the time-of-flight measurements, although the mechanism of response time difference is not clear. A similar difference in the response time was also observed for conventional  $\text{Ce}^{3+}$ -doped Li glass scintillation (Fairley & Spowart, 1978).

Based on these information, we show the feasibility of the custom-developed APLF80 + 3Pr scintillator material as a fast-response neutron detector for laser fusion diagnostics. The detection of ICF-originated neutrons was successfully carried out in laser fusion experiments at the GEKKO XII facility of the Institute of Laser Engineering, Osaka

University. In this study, a fusion target made from a deuterated plastic shell was irradiated by the 12 high-intensity Nd-glass lasers of the GEKKO XII facility. A detailed description of typical fusion experiment at GEKKO XII is described in (Azechi et al., 1991). As much as  $5 \times 10^5$  DD-fusion neutrons were observed using conventional neutron detectors, based on plastic scintillators. The fluorescence from the APLF80 + 3Pr sample that was positioned at about 10 cm from the fusion target was transmitted using a bundle optical fiber and detected by an ultraviolet photomultiplier as shown in Fig. 7. Taking into account the distance between the target and the APLF80+3Pr glass scintillator, and the difference of the time-of-flight of X-ray (30 cm/ns) and neutrons (2.2 cm/ns), the signal at round 10 ns in Fig. 8 was identified to be that of DD primal neutron. With decay time of about 80 ns, such clear discrimination between x-rays and neutrons in this short interval is impossible with traditional cerium doped lithium glass scintillators.

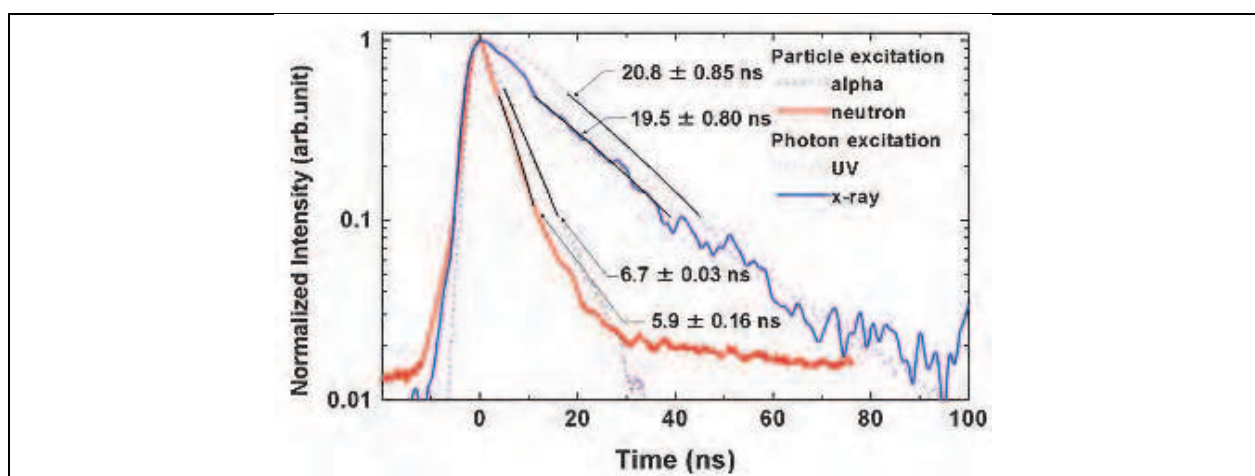


Fig. 6. The APLF+3Pr luminescence lifetime for alpha, neutron, x-ray, and UV pulse excitation. The lifetime varies from ~20 ns to under 7 ns, depending excitation source. This variation in the sample's decay time for different excitation energies suggests its capability to be used as detector in laser fusion time of flight experiments.

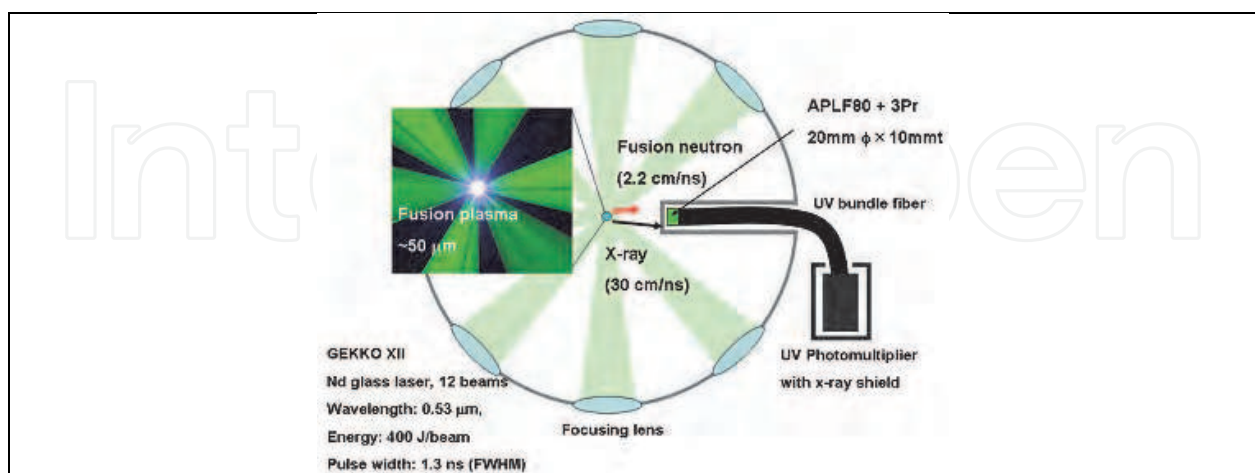


Fig. 7. Experimental set up of the time-of-flight experiment for the neutron detector. The detector is placed about 10 cm from the deuterated plastic target. The target is irradiated by 12 high energy beams of the GEKKO XII facility of the Institute of Laser Engineering, Osaka University.

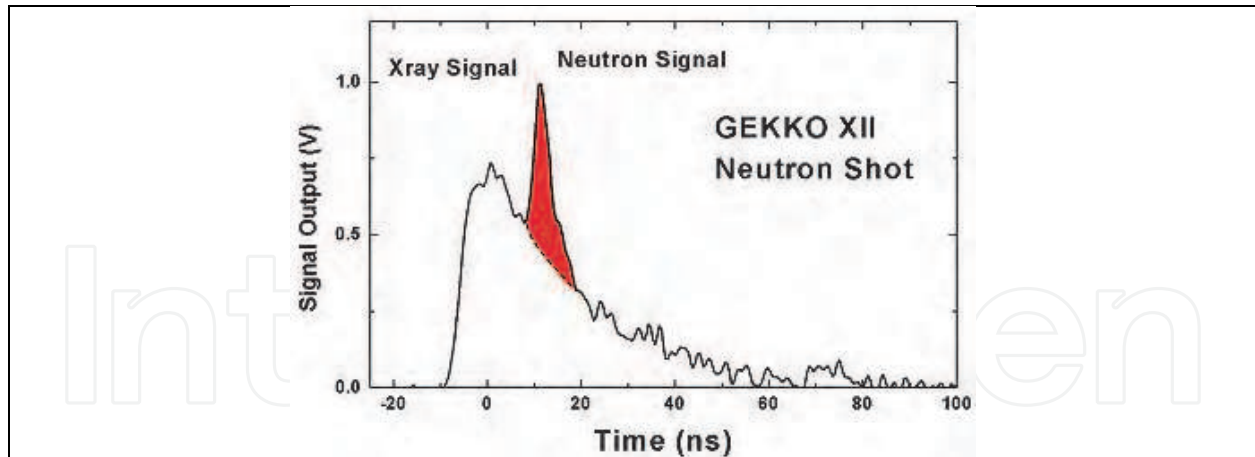


Fig. 8. The neutron signal at about 12 ns was successfully detected at the GEKKO XII facility fusion experiment.

## 5.2 Ce-doped fluoride

As mentioned in section 5.1,  ${}^6\text{Li}$  is known to have a large cross section for high-energy neutrons. This makes lithium-rich compounds prominent candidates for a host, especially when doped with a high quantum efficiency light emitting ion. Particularly, Li-rich fluorides are important hosts for these applications because of their relatively wide bandgap, which make them transparent even down to the vacuum ultraviolet region (below 200 nm). On the other hand, three trivalent ions are being considered as dopants, namely, Cerium ( $\text{Ce}^{3+}$ ), Praseodymium ( $\text{Pr}^{3+}$ ), and Neodymium ( $\text{Nd}^{3+}$ ) (van Eijk et al., 1994). Previously,  $\text{Nd}^{3+}:\text{LaF}_3$  (Nakazato et al., 2010a) and  $\text{Nd}^{3+}:\text{La}_x\text{Ba}_{(1-x)}\text{F}_{(3-x)}$  (Cadatal et al., 2007, 2008) have been reported as possible scintillator materials. However, of these three,  $\text{Ce}^{3+}$  has the smallest energy difference between the 4f and 5d levels, therefore resulting to a more efficient energy transfer to the dopant ion (van Eijk et al., 1994). The small energy difference also translates to a longer emission wavelength for  $\text{Ce}^{3+}$ -doped materials. A longer emission wavelength is advantageous because it can easily match the sensitivity of light sensors. For these reasons,  $\text{Ce}^{3+}:\text{LuLiF}_4$  (Ce:LLF) is explored as a viable scintillator material (Nakazato et al., 2010b). This material has been extensively investigated as a tunable ultraviolet laser medium and amplifier (Dubinskii et al., 1992; Sarukura et al., 1995a, 1995b, 1998).

For the development of scintillators, specifically for nuclear fusion applications, material optimization and doping concentration are extremely important. Material screening is typically accomplished through characterization of the material's response time for different neutron or photon excitation energies (M. Tanaka et al., 2007). However, since the short-pulse and high-energy neutron generated by nuclear fusion is not available on a daily basis; the free electron laser (FEL) can be an alternative excitation source for material screening. Moreover, the FEL provides flexibility in tunability and operation, therefore making it an important aide in accelerating material development. Among such FELs, the storage ring free-electron laser (SRFEL) is an appropriate choice because of its adequately high repetition rate, which is needed for the suitable evaluation of fluorescence decay times that are typically in the order of tens of nanoseconds (Hosaka et al., 2002). These decay times have been characteristically observed from  $\text{Ce}^{3+}$  doped fluorides.

In this section, Ce:LLF is reported as a fast scintillator using a SRFEL operating in the deep ultraviolet region. The response time is comparable to that of commercially available

scintillators, KG2 and GS2 (Saint-Gobain Crystals, 2007-2008). Fluorescence spectral and temporal profiles also seem to have a flat spectral response at each of its three excitation channels. This report is the first systematic study on Ce:LLF as a scintillator where SRFEL is also shown to be a powerful tool for material survey.

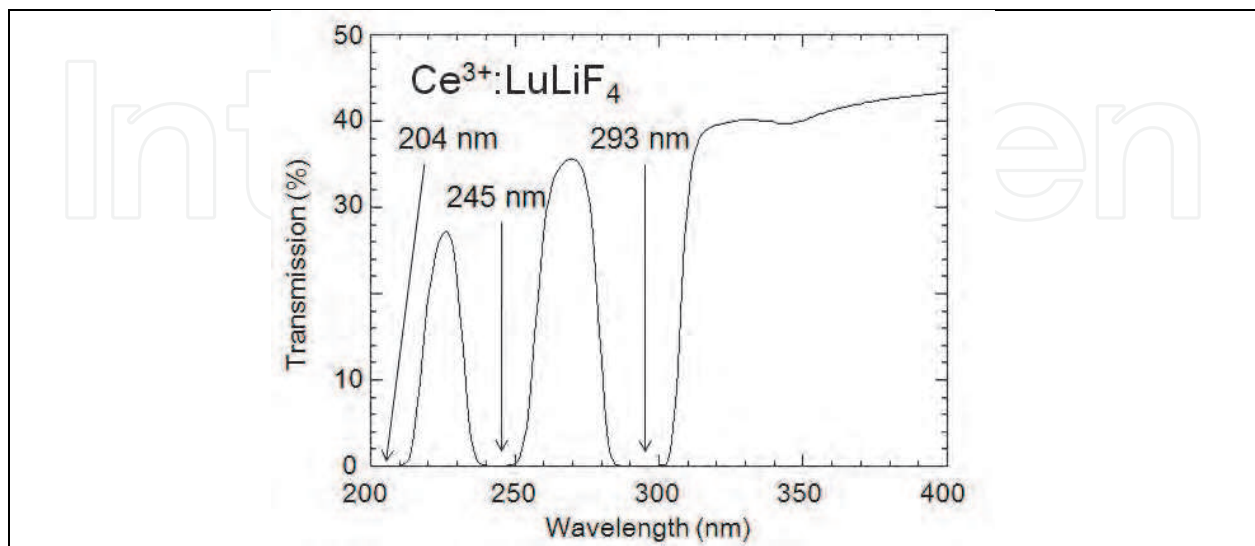


Fig. 9. Transmission spectrum of the 10 mm thick Ce:LLF. Central wavelength of the absorption bands are situated at around 204 nm, 245 nm, and 293 nm. The doping concentration of this material is 1mol%.

The Ce:LLF crystal used in our experiments contained 1mol% Ce<sup>3+</sup>. The crystal, which was grown by the Czochralski technique, was cut into a half-cylinder with dimensions of 18mm for the diameter of the semi-circle and 10 mm for the length. The crystal's c-axis is along its length, such that it is parallel to the direction of the excitation beam. All of the three flat surfaces were polished. Detailed specification of the Ce:LLF crystal used in this experiment is referred to in (Ranieri et al., 2000; Liu et al., 2000).

The experiment was carried out at the UVSOR facility of the Institute for Molecular Science. The SRFEL, which is parasitically installed at the BL5U beam line, was used as the excitation source. Wavelengths from 199 nm to 800 nm with a repetition rate of 11 MHz and pulse duration of 15 ps were available for material characterization (Zen et al., 2009). This wide range of tunability is advantageous for material characterization because it allows one to choose the excitation wavelength to match the absorption band of the material. For the case of Ce:LLF, the wavelength was consecutively tuned to 216 nm and 243 nm. As shown in Fig. 9, these wavelengths exactly match the absorption band of CeLLF. These well-defined bands can be attributed to 4f-5d transitions in Ce<sup>3+</sup>. The beam from the SRFEL was focused to the sample almost along the c-axis. A streak camera coupled to a spectrograph and a CCD camera was used to measure the time-resolved fluorescence spectra. The system has a spectral resolution of ~1 nm and a temporal resolution of ~9.4 ns. The spectral and temporal profile of the fluorescence spectra was also measured using the third harmonic (290 nm) of a Ti:Sapphire regenerative amplifier, for reference. The 290-nm emission of this laser system operated at a repetition rate of 1 KHz, a pulse energy of ~40 μJ, and a pulse duration of ~100 fs. All experiments were done at room temperature.

Fluorescence image, as captured by the streak camera, for the 243-nm excitation wavelength is shown in Fig. 10. Two spectra can be observed in this streak camera image. These are

fluorescence emissions from two consecutive excitation pulses. The 11 MHz repetition rate of the SRFEL meant that the sample is irradiated by one pulse every  $\sim 90$  ns. Therefore, two fluorescence emissions from two consecutive pulses were detected in one streak camera scan. This is also the case for the 216 nm excitation. We obtained the time-integrated fluorescence spectrum by integrating the signal over the time axis of the time-wavelength map of the streak camera data; and we found two fluorescence peaks, one at 308 nm and the other at 326 nm, as shown in Fig. 11 (blue line). These fluorescence peaks are consistent with previous reports (Sarukura et al., 1995; Ranieri et al., 2000; Rambaldi et al., 1998; Combes et al., 1997). The  $4f^{25}d$  excited state configuration of  $Ce^{3+}$  in a LLF host is split into four energy levels as a result of the  $S_4$  point symmetry at the  $Ce^{3+}$  site (Sarukura et al., 1995; Combes et al., 1997). The three absorption bands in Fig. 9 correspond to the three lowest energy levels of this  $4f^{25}d$  configuration with energies at  $\sim 32.9 \times 10^3$  to  $\sim 35.3 \times 10^3$   $cm^{-1}$  (304 to 283 nm),  $\sim 39.7 \times 10^3$  to  $\sim 40.6 \times 10^3$   $cm^{-1}$  (252 to 246 nm), and  $\sim 46.7 \times 10^3$  to  $\sim 50 \times 10^3$   $cm^{-1}$  (214 to  $\sim 200$  nm). The 308 nm ( $\sim 32.5 \times 10^3$   $cm^{-1}$ ) and 329 nm ( $\sim 30.4 \times 10^3$   $cm^{-1}$ ) emission peaks can therefore be attributed to radiative transitions from the lowest energy level of the  $4f^{25}d$  excited state configuration to the  ${}^2F_{5/2}$  ( $0$   $cm^{-1}$ ) and  ${}^2F_{7/2}$  ( $\sim 2 \times 10^3$   $cm^{-1}$ ) energy levels of the  $4f^3$  ground state configuration, respectively (Ehrlich et al., 1979). These energies are specified in the energy level diagram, shown in Fig. 12.

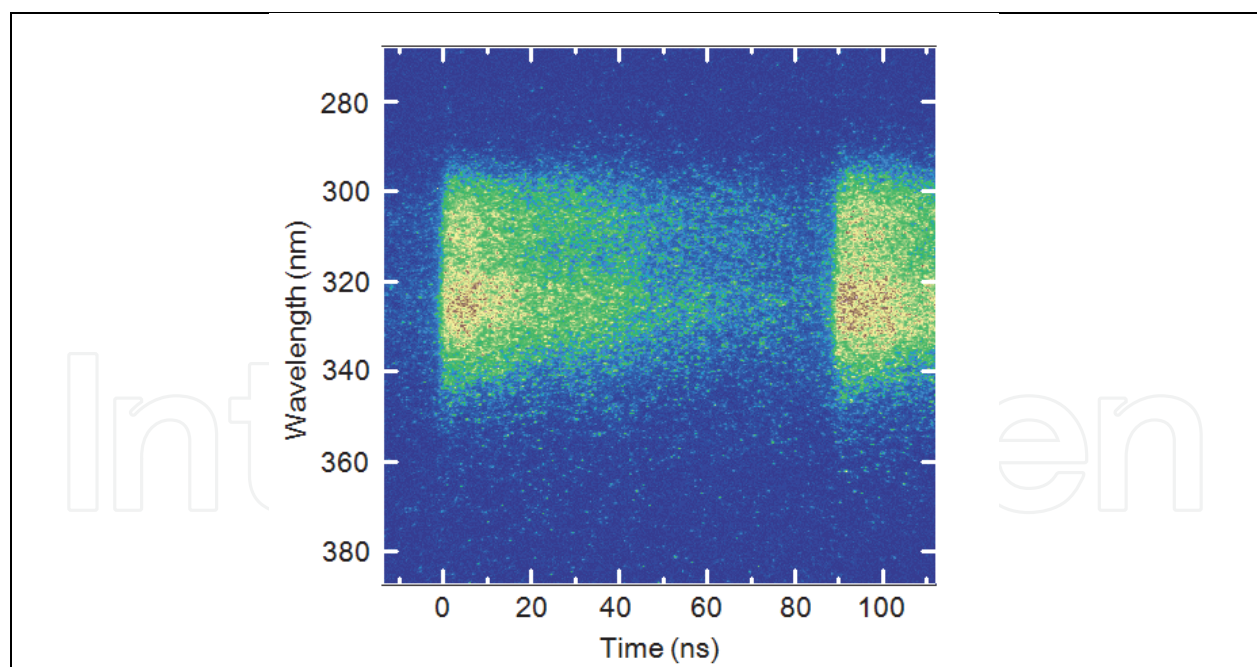


Fig. 10. Streak camera image of the Ce:LLF emission excited by the SRFEL tuned at 243 nm. The SRFEL had a repetition rate of 11 MHz, therefore two fluorescence images were captured by the 100-ns window of the streak camera.

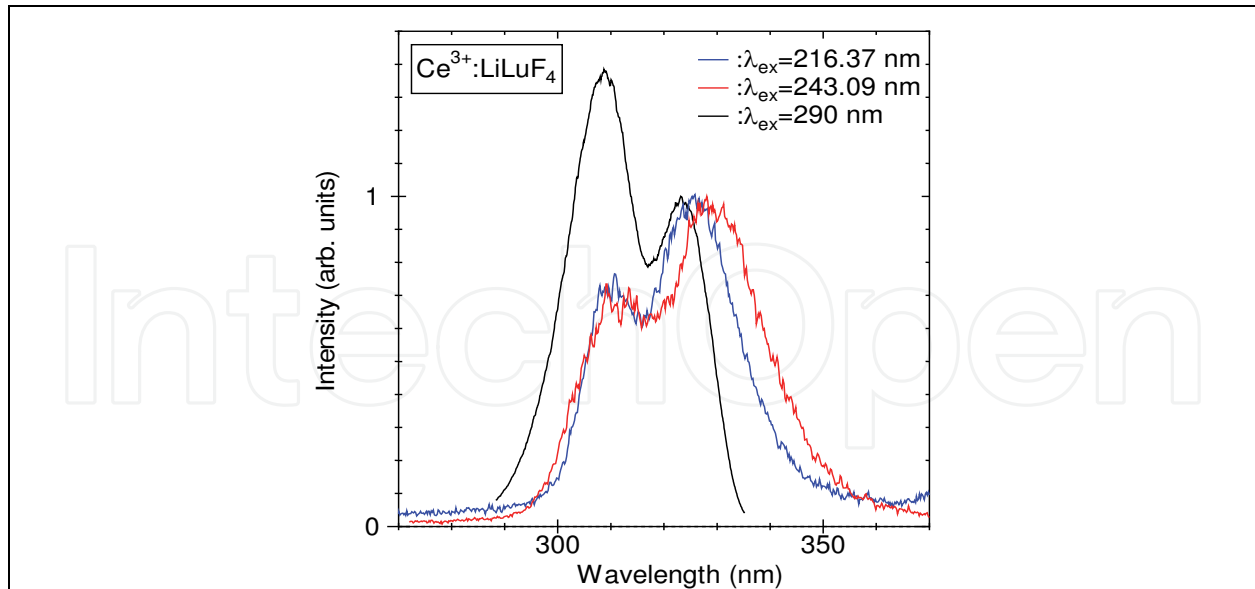


Fig. 11. Spectral profile of the fluorescence emission after consecutively exciting the three absorption channels of Ce:LLF with the SRFEL tuned at 243 nm and 216 nm and by the 290-nm emission of a Ti:sapphire laser. Transition from the  $4f^25d$  excited state configuration to the  $4f^3$  ground state configuration of  $Ce^{3+}$  resulted to two fluorescence peaks, one at 308 nm and the other at 329 nm.

Two peaks, 308 nm and 326 nm, were also observed for the 216 nm SRFEL excitation, as shown in Fig. 11 (blue line). Since the emission was also influenced by the  $Ce^{3+}$  doping, these fluorescence peaks were similar to the 243-nm excitation case wherein the fluorescence peaks were located at 308 nm and 329 nm where the transition was from the lowest energy level of the  $4f^25d$  excited state configuration to the  $^2F_{5/2}$  and  $^2F_{7/2}$  energy levels of the  $4f^3$  ground state configuration.

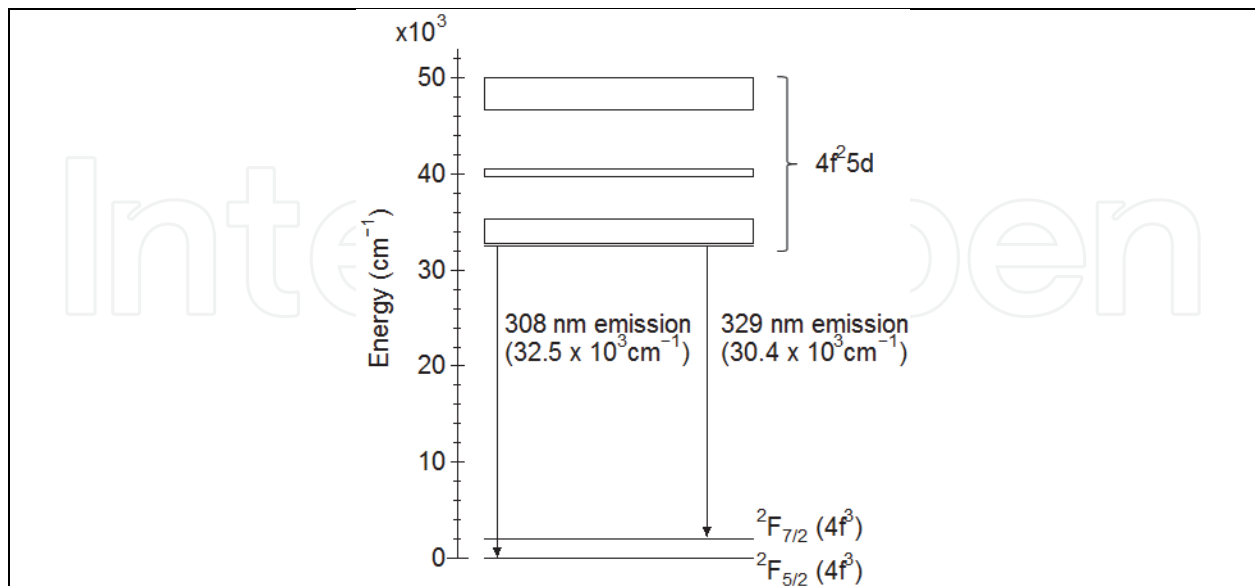


Fig. 12. Energy level diagram of  $Ce^{3+}$  in Ce:LLF. Two emission peaks originate from the transitions from the lowest  $4f^25d$  excited states to the  $^2F_{5/2}$  (308 nm emission) and  $^2F_{7/2}$  (329 nm emission).

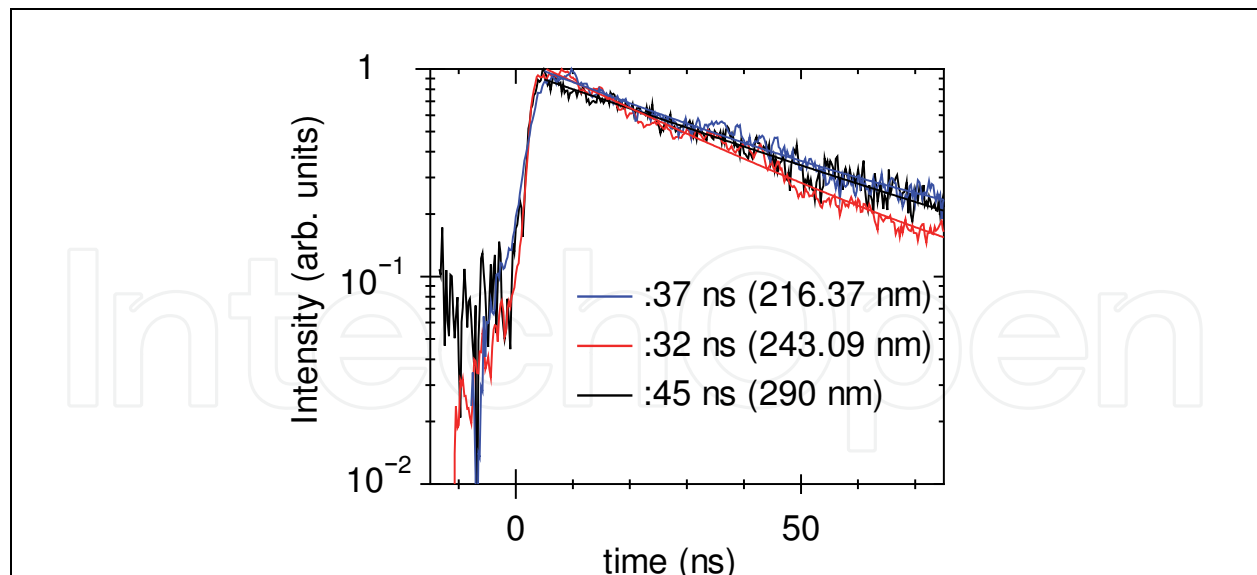


Fig. 13. Temporal profile showing fluorescence lifetimes for the 243 nm (SRFEL), 216 nm (SRFEL), and 290 nm (Ti:sapphire) excitation. These values are fast enough for ignition timing in fast-ignition, inertial confinement nuclear fusion using laser.

The fluorescence of the same sample was also measured when a 290-nm, fs excitation laser was used. The spectral profile is shown in Fig. 11 as well. Similar to the results of the SRFEL-excited fluorescence spectrum, peaks at 308 nm and 325 nm were observed. This similarity is indicative that the transitions brought about by the  $\text{Ce}^{3+}$  doping has a relatively flat spectral response across its absorption bands regardless of the excitation source, therefore making Ce:LLF as an attractive scintillator material for various excitation sources.

The fluorescence decay times for the three excitation wavelengths are shown in Fig. 13. The decay curves are single exponential with lifetimes of 32 ns, 37 ns, and 45 ns for the 243-nm, 216-nm, and 290-nm excitation wavelengths, respectively. The variation of these fluorescence decay times is less than the temporal resolution of the streak camera system, and thus within measurement uncertainty. The average value of the fluorescence decay time is  $\sim 40$  ns. The relatively flat spectral response across its absorption bands makes Ce:LLF a viable scintillator material for various short-wavelength excitation sources. The fluorescence decay time of commercial scintillators, for example KG2 or GS2, is  $\sim 40$  ns (Saint-Gobain Crystals, 2007-2008). Scintillation decay time of Ce:LLF might be a few ns slower, however, it is still acceptable for ignition timing in fast-ignition, inertial confinement nuclear fusion using laser.

### 5.3 Other scintillators

Fast scintillators, with response times in the nanosecond or even picosecond regime would play an important role in the advancement of radiation detection. For completeness, this section will discuss two solid-state materials that have been studied and have been shown to have potential as fast scintillators.

#### 5.3.1 Zinc oxide (ZnO)

The feasibility of ZnO crystal as a fast scintillator in the ultraviolet (UV) and extreme ultraviolet (EUV) region is reported. Over the past decade, ZnO has been intensively

studied as a light emitting diode and as a nanostructured material with improved optical properties (Cao & Du, 2007; Hauschild et al., 2006; Ichimiya et al., 2006; Jen et al., 2005; Ohta et al., 2000; Qian et al., 2007; Xu et al., 2007; Yu & Cardona, 2001; Zhang et al., 2007). In relation to this, the hydrothermal method is a novel growth method suitable for growing various crystals, including oxides such as ZnO. This method is capable of producing high-crystalline quality and large-sized homogeneous samples (Ohshima et al., 2004). The efficacy of a hydrothermal-method-grown ZnO crystal as a scintillator for UV region has been previously demonstrated (Furukawa et al., 2008; M. Tanaka et al., 2007; Nakazato et al., 2009), wherein the reported decay time of the ZnO scintillator was 1ns for EUV excitation at 13nm using Ag-plasma EUV laser. However, a faster response time is needed. In this section, an intentionally iron (Fe)-doped, hydrothermal-method-grown, ZnO crystal, is demonstrated to exhibit a response time faster by over one order of magnitude for soft x-ray pulsed excitation from the actual XFEL prototype (SPring-8 compact self amplification of spontaneous emission source [SCSS] test accelerator) at the SPring-8 research facility in RIKEN (Shimizu et al., 2010; Yamanoi et al., 2010).

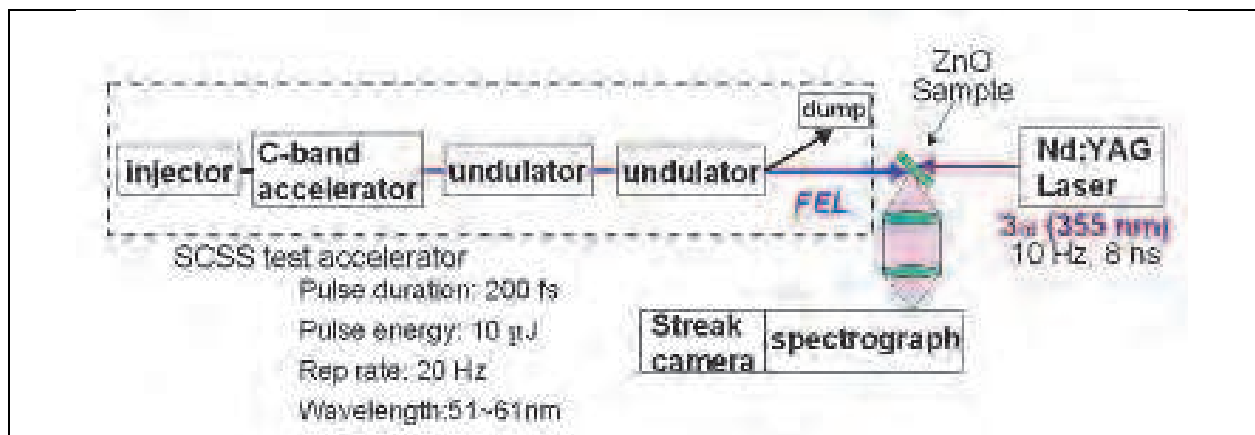


Fig. 14. Experimental setup for the measurement of the time resolved spectrum using the SCSS test accelerator (200-fs pulse duration, 10-μJ pulse energy, and 20-Hz repetition rate at 51–61nm). The sample was placed inside a vacuum chamber and excited by the EUV pulse from the SCSS test accelerator. The fluorescence was observed using a streak camera with the spectrograph.

The faster response time of the ZnO scintillator in this work was achieved by modifying the previously reported hydrothermal method ZnO crystal growth (Ohshima et al., 2004). The growth modification was aimed to introduce other fluorescence quenching channels by intentional doping during growth. To do this, the platinum lining of the crystal growth container was removed to facilitate the intentional doping of Fe-ion impurities. Three-dimensional-transition metals such as Fe in other semiconductor materials are known to play the role of lifetime-shortening impurity. The concentration of other impurities such as Li, K, and Al also increased, when the Pt lining was removed. However, the rate of increase in these metals is one order lower than that of Fe. Moreover, the contribution of these metals to the shortening of the lifetime is known to be smaller than that of transition metals. These results suggest that Fe is the main impurity. The sample was grown at a temperature of 300–400°C and at 80–100 MPa pressure and the crystal was cut at the (0001) surface orientation. The density of Fe-ion impurities in this sample was 0.61ppm, which is more than two orders of magnitude higher compared to previous ZnO samples grown with the Pt lining.

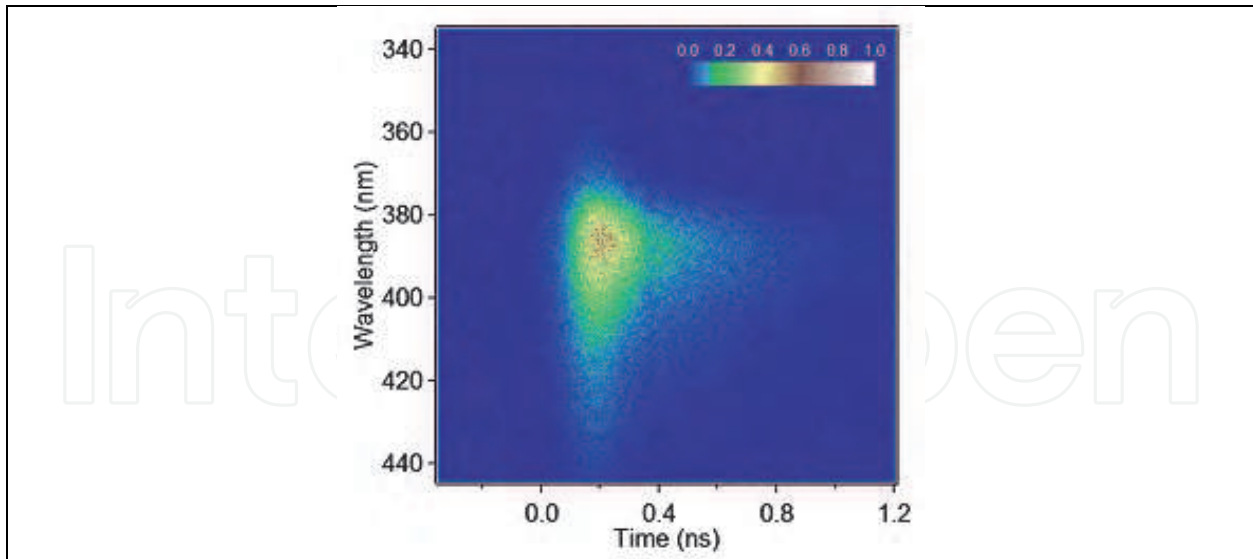


Fig. 15. Streak camera image of the fluorescence from ZnO. This is a 50000-shot integrated signal excited by 56 nm. The vertical axis is wavelength (nanometer) and the horizontal axis is time (nanosecond). The dominant fluorescence peak was centered at around 380 nm.

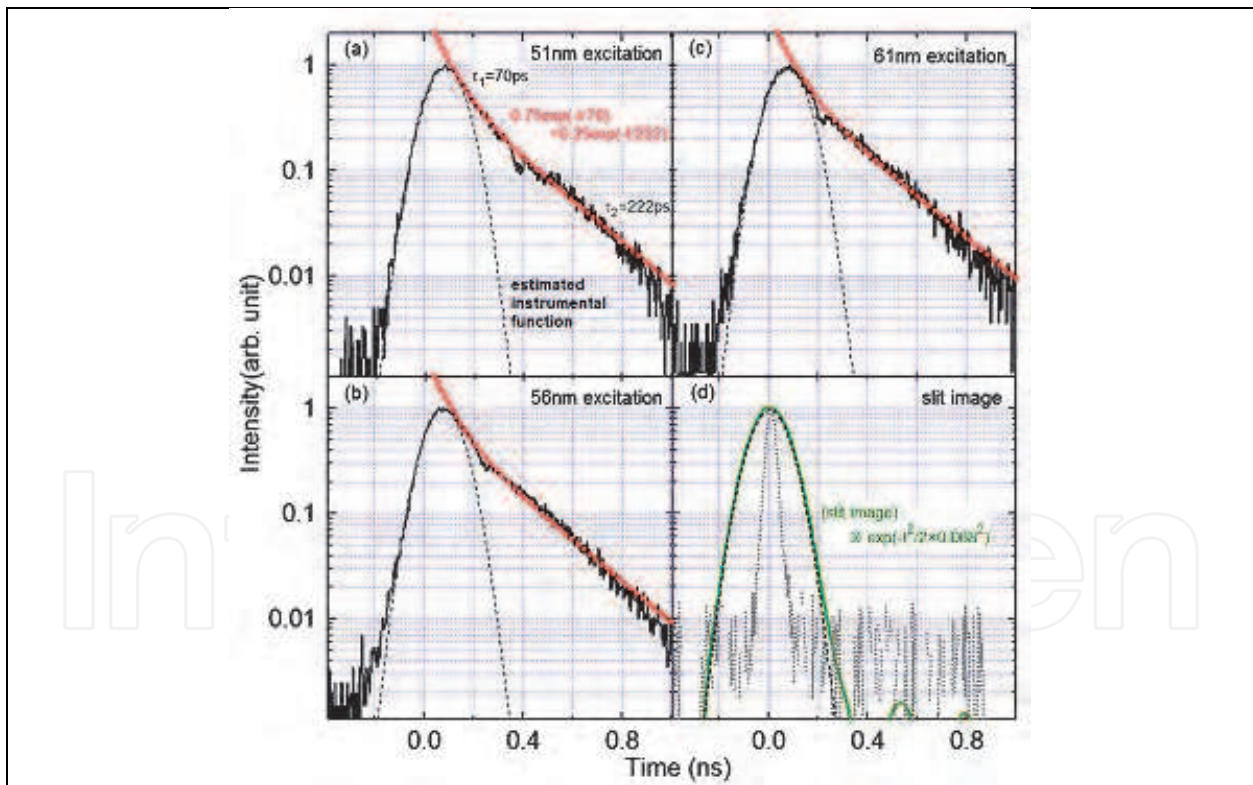


Fig. 16. Temporal profiles of the ZnO fluorescence excited by (a) 51nm, (b) 56nm, and (c) 61 nm. The observed profiles can be fitted by double exponential decays described as  $I = A_1 \exp(-t/\tau_1) + A_2 \exp(-t/\tau_2)$  (dotted line). The fitting parameters are  $A_1 = 0.75$ ,  $A_2 = 0.25$ ,  $\tau_1 = 70\text{ps}$ , and  $\tau_2 = 222\text{ps}$ . The estimated instrumental function was plotted with a dot line in each graph. (d) Slit image (dotted line) and a calculated curve of a convolution of the slit image and a normal distribution function (solid line).

Initially, the response time of Fe-ion doped ZnO scintillator was evaluated using the third harmonics of a mode-locked Ti:sapphire femtosecond laser at 290nm. The typical band-to-band ultraviolet fluorescence at 380nm was successfully observed, with a decay time of ~80ps. This is significantly faster compared with the previously reported 1-ns decay time for the 380-nm fluorescence of undoped ZnO. The 1x1cm<sup>2</sup>, 0.5-mm thick double-side polished ZnO crystal was mounted in a vacuum chamber, and the third harmonics of a neodymium-doped YAG (Nd:YAG) laser was initially used as excitation for alignment purposes. The sample was illuminated from the backside, in a counter propagation configuration with the beam path of the SCSS test accelerator, as shown in Fig. 14. The SCSS test accelerator having 200-fs pulse duration, 10-μJ pulse energy, and 20-Hz repetition rate, was focused by an oblique mirror (Mimura et al., 2008). With a mirror focal length of 1m, the spot size at the focus was about 20 μm. To minimize the risk of damage, however, the sample was placed 5 cm away from focus, and the radius of the beam at this location was estimated to be 500 μm. The emission wavelength of the SCSS test accelerator can be tuned from 51 to 61 nm. Fluorescence was collected and focused to the entrance slit of a spectrograph using quartz lenses. The fluorescence spectrum and the lifetime of the ZnO sample were measured using a 25-cm focal-length spectrograph (groovedensity 600gr/mm) coupled to a streak camera unit (HAMAMATSUC1587) and a charge coupled device camera.

The ZnO fluorescence, excited by light pulses of the SCSS test accelerator at 51, 56, and 61 nm with 50000 shots was measured using the spectrograph coupled to the streak camera system. Figure 15 shows the streak camera image of the fluorescence using 56-nm excitation from the SCSS test accelerator. The dominant fluorescence peak was centered at around 380 nm (Chen et al., 2000). The temporal profiles of this image at 51-, 56-, and 61-nm excitation are shown in Figs. 16(a)–10(c), respectively. The measured decay profiles can be well-fitted to a double exponential decay with time constants of 70 and 222 ps for the fast and slow decay-time constants, respectively. These two decay constants have been previously reported in several works involving UV-excited ZnO single crystals, where the fast decay time is attributed to the lifetime of free excitons, while the slower decay time is assigned to trapped carriers (Wilkinson et al., 2004). This measured response time is currently the fastest for a scintillator operating in the 50–60 nm region. In addition, the fluorescence intensity and time decay profile appears to be independent of the excitation wavelength within the 50–60 nm range. This flat response makes the Fe-doped ZnO scintillator ideal for operation both for UV and in soft x-ray excitation schemes.

### 5.3.2 Neodymium-doped lanthanum fluoride (Nd<sup>3+</sup>:LaF<sub>3</sub>)

Scintillators in the vacuum ultraviolet (VUV) region are continuously being developed for various applications. In this section, the scintillation properties of Nd<sup>3+</sup>:LaF<sub>3</sub> is discussed. Characterization was performed by exciting the sample with the third harmonics of a Ti:sapphire regenerative amplifier having 1-KHz repetition rate, 10-μJ pulse energy, and 200-fs pulse duration. The excitation wavelength in this case is at 290 nm; while the reported fluorescence wavelength of Nd<sup>3+</sup>:LaF<sub>3</sub> is at 175 nm. With the unavailability of ultrashort-pulse EUV sources, we attempt to demonstrate the scintillation properties of this crystal for ultrafast excitation using possibly a multiphoton process. Spectroscopic studies have revealed that the absorption edge of this crystal is at ~168 nm (Nakazato et al., 2010a).

Pulses were focused by a 20-cm lens onto the sample inside a vacuum chamber. A VUV spectrometer and streak camera system was used to evaluate fluorescence from this sample.

The streak camera image of fluorescence is shown in Fig. 17 (a). The streak camera image of the 290-nm, fs excitation is also shown in the same figure as Fig. 17 (b) for reference. On the other hand, the spectral and temporal profile obtained by sweeping across the vertical axis is shown in Fig. 18. The fluorescence peak is centered at around 175 nm with a decay time of about 7.1 ns.

The absorption spectrum of the sample from 200 to 400 nm revealed the presence of multiple absorption bands, particularly at 290 nm. Moreover, the slope of fluorescence intensity as a function of pump fluence was experimentally verified to be equal to unity. In this aspect, frequency up-conversion by energy transfer could have been the governing mechanism [3], owing to the absorption band at 290 nm. Since fluorides have low phonon energies, the lifetimes of intermediate levels are long enough (order of  $\mu\text{s}$ ) for the accumulation of electrons in an intermediate excited state. Existing solid-state, inorganic scintillators in the ultraviolet region typically have decay times of a few tens of nanoseconds. As such, the  $\text{Nd}^{3+}:\text{LaF}_3$  fluorescence decay time of about 7.1 ns would be among the fastest solid-state, inorganic scintillators.

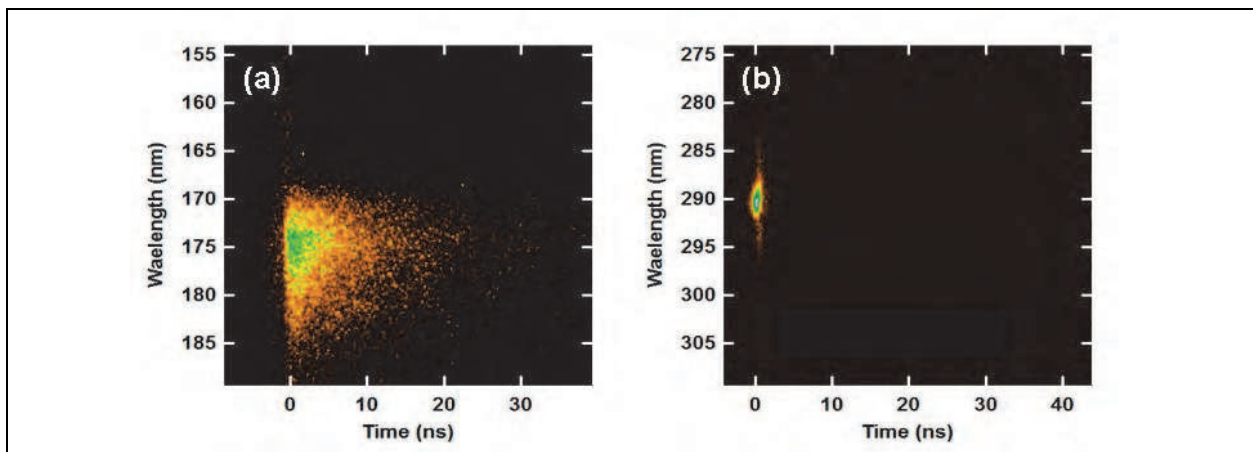


Fig. 17. (a) Streak camera image of fluorescence from a cuboid  $\text{Nd}^{3+}:\text{LaF}_3$  excited by 290-nm femtosecond pulses shown in (b).

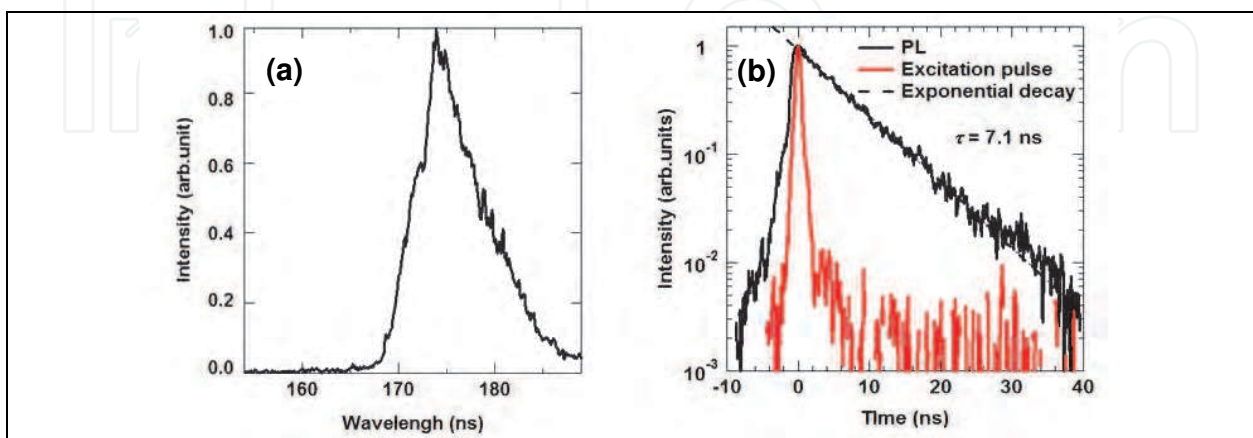


Fig. 18. (a) Spectral and (b) temporal profiles of the fluorescence shown in Fig. 17 (a).

## 6. Conclusion

In the field of fusion research, understanding the plasma dynamics could very well be the key in feasibly attaining controlled fusion. The time-resolved fluorescence spectra of Ce:LLF when excited by SRFEL tuned at 243 nm and 216 nm and by the 290-nm emission of a Ti:sapphire laser were measured to determine the feasibility of using this material as a scintillator for fast-ignition laser fusion. Two peaks were observed, one at 308 and another at 329 nm, which can be attributed to transitions from the lowest energy level of the  $4f^{25}d$  excited state configuration to one of the two energy levels in the  $4f^3$  ground state configuration of  $Ce^{3+}$ . The relatively flat spectral and temporal response across its absorption bands makes Ce:LLF an attractive scintillator material for various excitation sources. Scintillation decay time of Ce:LLF might be few ns slower, however, it is still acceptable for measurements of ignition timing in fast-ignition, inertial confinement nuclear fusion using laser.

In response to the need for a fast-response scintillator for precise time-resolved radiation measurement, we have succeeded in developing a fast-response  $^6Li$  glass scintillator material suitable for scattered neutron diagnostics of the ICF plasma, with a response time of about 20 ns. Using this custom-developed material, fusion-originated neutrons were successfully observed using the GEKKO XII laser at the Institute of Laser Engineering, Osaka University. These results could pave the way for a new class of scintillator devices, optimized for neutron detection. In particular, after proper growth and device design considerations are carried out, future discrimination between primary and low-energy scattered neutrons using this material could be realized.

Due to the increasing demand for scintillators with fast response time, several materials are currently being investigated. In this aspect, vacuum ultraviolet fluorescence from a  $Nd^{3+}:LaF_3$  crystal excited by 290 nm femtosecond pulses from a Ti:sapphire laser is reported. Peak emission at 175 nm with 7 ns lifetime is observed. This decay time would be one of the fastest among fluoride scintillators. On the other hand, a hydrothermal-method grown ZnO scintillator exhibited an over one-order of magnitude faster response time by intentional Fe ion doping. The rise and decay time constants of the fluorescence are measured to be less than 10 ps and 100 ps, respectively. Its fluorescence is also sufficiently bright to be detected by a streak-camera system even in single shot mode without any accumulation.

Meanwhile, mapping of radiation sources is very useful to detect and characterize invisible radiation accidents and/or radioactive contamination. For this purpose, bundles composed of well-designed and regularly arranged scintillation fiber-segments or thin cylinders have been developed to detect and display the radiation sources as a map, using the directional sensitivity of the segments or cylinders for locating sources of incident radiation. In this case, the more important attribute would be scintillation intensity, regardless of decay time, since available moving picture systems are usually 30 frames per second. A bundle composed of several kinds of thin cylinder or fiber segment scintillators has appropriate sensitivity for several kinds of incident radiation and thus serves as a panchromatic detector; whereas a bundle made from a single type of scintillator functions as a monochromatic detector. By combining several types of scintillating elements into a bundle, we have developed a “panchromatic” detector that is suitable for use against radiation from different types of sources.

## 7. Acknowledgment

Work on  $Pr^{3+}$ -doped glass scintillator was supported by the Japan Society for the Promotion of Science under the contracts of Grant-in-Aid for Scientific Research (S) (GrantNo.18106016),

Grant-in-Aid on Priority Area (GrantNo.16082204), Open Advanced Research Facilities Initiative, and Research Fellowship for Young Scientists (GrantNo.3273).

Work on Ce:LLF was in part performed by auspice of MEXT Japanese Ministry of Education, Culture, Sports, Science, and Technology project on "Development of Growth Method of Semiconductor Crystals for Next Generation Solid-State Lighting" and "Mono-energetic quantum beam science with PW lasers" and Scientific Research Grant-in Aid (17656027) from the MEXT. The results were achieved under the joint research project of the Institute of Laser Engineering at Osaka University, Extreme Photonics project from the Institute for Molecular Science.

For the work on ZnO, we are also grateful to the SCSS Test Accelerator Operation Group at RIKEN for continuous support in the course of the studies and Fukuda Crystal Laboratory for support in sample preparation.

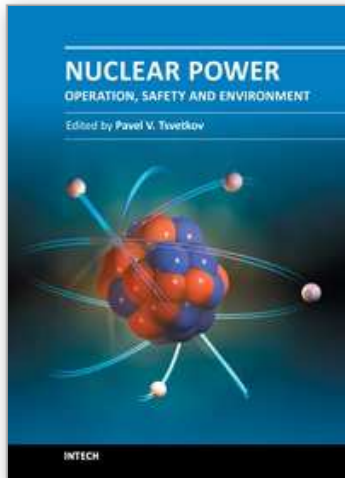
## 8. References

- Arikawa, Y., Yamanoi, K., Nakazato, T., Estacio, E. S., Shimizu, T., Sarukura, N., Nakai, M., Norimatsu, T., Azechi, H., Murata, T., Fujino, S., Yoshida, H., Kamada, K., Usuki, Y., Suyama, T., Yoshikawa, A., Sato, N., & Kan, H. (2009), Pr<sup>3+</sup>-doped fluoro-oxide lithium glass as scintillator for nuclear fusion diagnostics, *Review of Scientific Instruments*, Vol. 80, Issue 11, (November 2009), pp. 113504-113504-4, ISSN: 0034-6748
- Azechi, H., Jitsuno, T., Kanabe, T., Katayama, M., Mima, K., Miyanaga, N., Nakai, M., Nakai, S., Nakaishi, H., Nakatsuka, M., Nishiguchi, A., Norrays, P. A., Setsuhara, Y., Takagi, M., & Yamanaka, M. (1991). High-density compression experiments at ILE, Osaka, *Laser and Particle Beams*, Vol. 9, Issue 2, (June 1991), pp.193-207, ISSN: 0263-0346
- Cadatal, M., Seo, Y.S., Ono, S., Furukawa, Y., Estacio, E., Murakami, H., Fujimoto, Y., Sarukura, N., Nakatsuka, M., Suyama, T., Fukuda, K., Simura, R., & Yoshikawa, A. (2007), Nd<sup>3+</sup>:(La<sub>1-x</sub>Ba<sub>x</sub>)F<sub>3-x</sub> Grown by Micro-Pulling Down Method as Vacuum Ultraviolet Scintillator and Potential Laser Material, *Japanese Journal of Applied Physics*, Vol. 46, No. 40, (October 2007), pp. L985-L987, ISSN: 0021-4922
- Cadatal, M., Furukawa, Y., Seo, Y. S., Ono, S., Estacio, E., Murakami, H., Fujimoto, Y., Sarukura, N., Nakatsuka, M., Fukuda, K., Simura, R., Suyama, T., Yoshikawa, A., & Saito, F. (2008), Vacuum ultraviolet optical properties of a micro pulling-down-method grown Nd<sup>3+</sup>:(La<sub>0.9</sub>Ba<sub>0.1</sub>)F<sub>2.9</sub>, *Journal of the Optical Society of America B*, Vol. 25, No. 7 (July 2008), pp. B27-B31, ISSN: 0740-3224
- Cheon, M. S., Pac, S., Lee, F. G., Bertalot, L., & Walker, C. (2008). In-vessel design of ITER diagnostic neutron activation system, *Review of Scientific Instruments*, Vol. 79, Issue 10, (October 2008), pp.10E505-10E505-3, ISSN: 0034-6748
- Combes, C. M., Dorenbos, P., van Eijk, C. W. E., Pedrini, C., DenHartog, H. W., Gesland, J. Y., & Rodnyi, P. A. (1997). Optical and scintillation properties of Ce<sup>3+</sup> doped LiYF<sub>4</sub> and LiLuF<sub>4</sub> crystals, *Journal of Luminescence*, Vol. 71, Issue 1, (January 1997), pp. 65-70, ISSN: 0022-2313
- Dubinskii, M.A., Abdulsabirov, R.Y., Korableva, S.L., Naumov, A.K., & Semashko, V.V. (1992). New solid-state active medium for tunable ultraviolet lasers, *Proceedings of the 18th International Quantum Electronics Conference*, Moscow, Russia, June 1992

- Ehrlich, D., Moulton, P., & Osgood, R. (1979). Ultraviolet solid-state Ce:YLF laser at 325 nm, *Optics Letters*, Vol. 4, Issue 6, (Jun 1979), pp. 184-186, ISSN: 0146-9592
- Fairley, E. J. & Spowart, A. R. (1978). Neutron Scintillating Glasses Part Iii Pulse Decay Time Measurements At Room Temperature, *Nuclear Instruments and Methods*, Vol. 150, Issue 2, (April 1978), pp. 159-163, ISSN: 0168-9002
- Fukuda, T. & Chani, V. I. (2007). In: *Shaped Crystals*, Tsuguo Fukuda & Valery I.Chani, pp. , Springer-Verlag, ISBN: 978-3-540-71294-7, Berlin Heidelberg New York
- Fukuda, T., Rudolph, P. & Uda, S. (2004). In: *Fiber Crystal Growth from Melt*, Tsuguo Fukuda Peter Rudolph Satoshi Uda, pp. ,Springer-Verlag, ISBN: 3-540-40596-8, Berlin Heidelberg New York
- Glebov, V. Yu., Meyerhofer, D. D., Sangster, T. C., Stoeckl, C., Roberts, S., Barrera, C. A., Celeste, J. R., Cerjan, C. J., Dauffy, L. S., Eder, D. C., Griffith, R. L., Haan, S. W., Hammel, B. A., Hatchett, S. P., Izumi, N., Kimbrough, J. R., Koch, J. A., Landen, O. L., Lerche, R. A., MacGowan, B. J., Moran, M. J., Ng, E. W., Phillips, T. W., Song, P. M., Tommasini, R., Young, B. K., Caldwell, S. E., Grim, G. P., Evans, S. C., Mack, J. M., Sedillo, T. J., Wilke, M. D., Wilson, D. C., Young, C. S., Casey, D., Frenje, J. A., Li, C. K., Petrasso, R. D., Séguin, F. H., Bourgade, J. L., Disdier, L., Houry, M., Lantuejoul, I., Landoas, O., Chandler, G. A., Cooper, G. W., Leeper, R. J., Olson, R. E., Ruiz, C. L., Sweeney, M. A., Padalino, S. P., Horsfield, C., & Davis, B. A. (2006). Development of nuclear diagnostics for the National Ignition Facility (invited), *Review of Scientific Instruments*, Vol. 77, Issue 10, (October 2006), pp. 10E715-1-10E715-7, ISSN: 0034-6748
- Hosaka, M., Koda, S., Katoh, M., Yamazaki, J., Hayashi, K., Takashima, K., Gejo, T., & Hama, H. (2002). From the operation of an SRFEL to a user facility, *Nuclear Instruments and Methods in Physics Research Section A: Accelerators, Spectrometers, Detectors and Associated Equipment*, Vol. 483, Issues 1-2, (May 2002), pp. 146-151, ISSN: 0168-9002
- Ishii, M. & Kobayashi M. (1991). Single crystals for radiation detectors. *Progress in Crystal Growth and Characterization*, Vol. 23, (1992), pp. 245-311, ISSN: 0960-8974
- Izumi, N., Lerche, R. A., Phillips, T. W., Schmid, G. J., Moran, M. J., Koch, J. A., Azechi, H., & Sangster, T. C. (2002). Development of a gated scintillation fiber neutron detector for areal density measurements of inertial confinement fusion capsules, *Review of Scientific Instruments*, Vol. 74, Issue 3, (March 2003), pp. 1722-1725, ISSN: 0034-6748
- Kobayashi, M & Ishii, M. (2007). Chapter 7 Phosphors for X-ray and ionizing radiation, In: *Phosphor handbook*, William M. Yen , Shigeo Shionoya & Hajime Yamamoto, pp. 619-633, CRC Press, ISBN 978-084-9335-64-8, Florida, USA
- Lerche, R. A., Phillion, D. W., & Tietbohl, L. (1994). 25 ps neutron detector for measuring ICF-target burn history, *Review of Scientific Instruments*, Vol. 66, Issue 1, (January 1995), pp. 933 - 935, ISSN: 0034-6748
- Liu, Z., Shimamura, K., Nakano, K., Mujilatu, N., Fukuda, T., Kozeki, T., Ohtake, H., & Sarukura, N. (1999). Direct Generation of 27-mJ, 309-nm Pulses from a Ce<sup>3+</sup>:LiLuF<sub>4</sub> Oscillator Using a Large-Size Ce<sup>3+</sup>:LiLuF<sub>4</sub> Crystal, *Japanese Journal of Applied Physics*, Vol. 39, No. 2A, (February 2000), pp. L88-L89, ISSN: 0021-4922
- Murata, T., Fujino, S., Yoshida, H., Arikawa, Y., Nakazato, T., Shimizu, T., Sarukura, N., Nakai, M., Norimatsu, T., Azechi, H., Kamada, K., Usuki, Y., Suyama, T., Yoshikawa, A., Sato, N., & Kan, H. (2010). Custom-Designed Fast-Response Praseodymium-Doped Lithium 6 Fluoro-Oxide Glass Scintillator With Enhanced

- Cross-Section for Scattered Neutron Originated From Inertial Confinement Fusion, *IEEE Transactions on Nuclear Science*, Vol. 57, No. 3, (June 2010), pp. 1426-1429, ISSN: 0018-9499
- Nakazato, T., Cadatal-Raduban, M., Furukawa, Y., Pham, M., Estacio, E., Shimizu, T., Sarukura, N., Fukuda, K., Suyama, T., Yanagida, T., Yokota, Y., Yoshikawa, A., & Saito, F. (2010), Nd<sup>3+</sup>:LaF<sub>3</sub> as a Step-Wise Excited Scintillator for Femtosecond Ultraviolet Pulses, *IEEE Transactions On Nuclear Science*, Vol. 57, Issue 3, (June 2010), pp. 1208-1210, ISSN: 0018-9499
- Nakazato, T., Furukawa, Y., Cadatal-Raduban, M., Pham, M., Tatsumi, T., Saiki, A., Arikawa, Y., Sarukura, N., Nishimura, H., Azechi, H., Mima, K., Fukuda, T., Hosaka, M., Katoh, M., & Kosugi, N. (2010), Systematic Study on Ce:LuLiF<sub>4</sub> as a Fast Scintillator Using Storage Ring Free-Electron Lasers, *Japanese Journal of Applied Physics*, Vol. 49, No. 12, (December 2010), pp. 122602-122602-4, ISSN: 0021-4922
- Ogawa, T. (2007). Patent Application PCT/JP2007/062817
- Ogawa, T., Sarukura, N., Watanabe, M., Fukuda, T., Nango, N. (2010), Two dimensional imaging of radiation accidents and radioactive contamination, *Optical Materials*, Vol. 32, Issue 7, (May 2010), pp. 753-755, ISSN: 0925-3467
- Petrizzi, L., Barnsley, R., Bertalot, L., Esposito, B., Haskell, H., Mainardi, E., Marocco, D., Podda, S., Walker, C., & Villari, S. (2007). Neutronic design of the ITER radial neutron camera, *Fusion Engineering and Design*, Vol. 82, Issues 5-14, (October 2007), pp.1308-1314, ISSN: 0920-3796
- Rambaldi, P., Moncorge, R., Wolf, J. P., Pedrini, C., & Gesland, J. Y. (1998). Efficient and stable pulsed laser operation of Ce:LiLuF<sub>4</sub> around 308 nm, *Optics Communications*, Vol. 146, Issues 1-6, (January 1998), pp. 163-166, ISSN: 0030-4018
- Ranieri, I. M., Shimamura, K., Nakano, K., Fujita, T., Liu, Z., Sarukura, N., & Fukuda, T. (2000). Crystal growth of Ce : LiLuF<sub>4</sub> for optical applications, *Journal of Crystal Growth*, Vol. 217, Issue 1-2, (July 2000), pp. 151-156, ISSN: 0022-0248
- Ress, D., Lerche, R. A., Ellis, R. J., & Lane, S. M. (1988). Neutron imaging of inertial confinement fusion targets at Nova, *Review of Scientific Instruments*, Vol. 59, Issue 8, (August 1988), pp. 1694-1696, ISSN: 0034-6748
- Saint-Gobain Ceramics & Plastics, Inc. (2007-2008). Lithium glass scintillators, In: *Saint-Gobain Ceramics & Plastics, Inc.*, March 4, 2011, Available from: <<http://www.detectors.saint-gobain.com/Lithium-Glass-Scintillator.aspx>>
- Sarukura, N., Dubinskii, M.A., Liu, Z., Semashko, V.V., Naumov, A.K., Korableva, S.L., Yu Abdulsabirov, R., Edamatsu, K., Suzuki, Y., Itoh, T., & Segawa, Y. (1995). Ce<sup>3+</sup>-activated fluoride crystals as prospective active media for widely tunable ultraviolet ultrafast lasers with direct 10-ns pumping, *IEEE Journal of Selected Topics in Quantum Electronics*, Vol. 1, Issue 3, (September 1995), 792-804, ISSN: 1077-260X
- Sarukura, N., Liu, Z., Segawa, Y., Edamatsu, K., Suzuki, Y., Itoh, T., Semashko, V. V., Naumov, A. K., Korableva, S. L., Abdulsabirov, R. Yu., & Dubinskii, M. A. (1995), Ce<sup>3+</sup>:LuLiF<sub>4</sub> as a broadband ultraviolet amplification medium, *Optics Letters*, Vol. 20, No. 3 (February 1995), pp. 294-296, ISSN: 0146-9592
- Sarukura, N., Liu, Z., Izumida, S., Dubinskii, M.A., Abdulsabirov, R.Y., Korableva, A.K., & Stella, L. (1998) All-Solid-State Tunable Ultraviolet Subnanosecond Laser with Direct Pumping by the Fifth Harmonic of a Nd:YAG laser, *Applied Optics*, Vol. 37, Issue 27, (September 1998), pp. 6446-6448, ISSN: 1559-128X

- Shimizu, T., Yamamoi, K., Estacio, E., Nakazato, T., Sakai, K., Sarukura, N., Ehrentraut, D., Fukuda, T., Nagasono, M., Togashi, T., Higashiya, A., Yabashi, M., Ishikawa, T., Ohashi, H., & Kimura H. (2010), Response-time improved hydrothermal-method-grown ZnO scintillator for soft x-ray free-electron laser timing-observation, *Review of Scientific Instruments*, Vol. 81, Issue 3, (March 2010), pp. 033102-1-033102-4, ISSN: 0034-6748
- Suzuki, Y., Kozeki, T., Ono, S., Murakami, H., Ohtake, H., Sarukura, N., Nakajyo, T., Sakai, F., & Aoki, Y. (2002). Hybrid time-resolved spectroscopic system for evaluating laser material using a table-top-sized, low-jitter, 3-MeV picosecond electron-beam source with a photocathode, *Applied Physics Letters*, Vol. 80, Issue.18, (May 2002), pp. 3280-3282, ISSN: 0003-6951
- Tanaka, K. A., Kodama, R., Kitagawa, Y., Kondo, K., Mima, K., Azechi, H., Chen, Z., Fujioka, S., Fujita, H., Johzaki, T., Lei, A., Matsuoka, T., Miyanaga, N., Nagai, K., Nagatomo, H., Nishimura, H., Norimatsu, T., Shigemori, K., Shiraga, H., Tanpo, M., Tohyama, Y., Yabuuchi, T., Zheng, J., Izawa, Y., Norreys, P. A., Stephens, R., & Hatchett, S. (2004). Progress and perspectives of fast ignition, *Plasma Physics And Controlled Fusion*, Vol. 46, No. 12B, (December 2004), pp. B41-B49, ISSN: 0741-3335
- Van Eijk, C.W.E., Andriessen, J., Dorenbos, P., Visser, R. (1994). Ce<sup>3+</sup> doped inorganic scintillators, *Nuclear Instruments and Methods in Physics Research Section A: Accelerators, Spectrometers, Detectors and Associated Equipment*, Vol. 348, Issues 2-3, (September 1994), pp. 546-550, ISSN: 0168-9002
- Yamanoi, K., Sakai, K., Nakazato, T., Estacio, E., Shimizu, T., Sarukura, N., Ehrentraut, D., Fukuda, T., Nagasono, M., Togashi, T., Matsubara, S., Tono, K., Yabashi, M., Kimura, H., Ohashi, H., Ishikawa, T. (2010), Response-time improved hydrothermal-method-grown ZnO scintillator for XFEL timing-observation, *Optical Materials*, Vol. 32, Issue 10, (August 2010), pp.1305-1308, ISSN: 0925-3467
- Yoshikawa, A., Kamada, K., Saito, F., Ogino, H., Itoh, M., Katagiri, T., Iri, D., & Fujita, M. (2008). Energy Transfer to Pr<sup>3+</sup> Ions in Pr:Lu<sub>3</sub>Al<sub>5</sub>O<sub>12</sub> (LuAG) Single Crystals, *IEEE Transactions on Nuclear Science*, Vol. 55, No. 3, (June 2008), pp.1372-1375, ISSN: 0018-9499
- Zen, H., Adachi, M., Hayashi, K., Katoh, M., Yamazaki, J., Tanikawa, T., Hosaka, M., Koike, M., Taira, Y., Uno, Y., & Yamamoto, N. (2009). Design Study of THz & VUV Coherent Source by Laser Seeding at UVSOR-II, *Proceedings of Free Electron Laser (FEL) Conference 2009, Liverpool, UK, August 2009*



## **Nuclear Power - Operation, Safety and Environment**

Edited by Dr. Pavel Tsvetkov

ISBN 978-953-307-507-5

Hard cover, 368 pages

**Publisher** InTech

**Published online** 06, September, 2011

**Published in print edition** September, 2011

Today's nuclear reactors are safe and highly efficient energy systems that offer electricity and a multitude of co-generation energy products ranging from potable water to heat for industrial applications. At the same time, catastrophic earthquake and tsunami events in Japan resulted in the nuclear accident that forced us to rethink our approach to nuclear safety, design requirements and facilitated growing interests in advanced nuclear energy systems, next generation nuclear reactors, which are inherently capable to withstand natural disasters and avoid catastrophic consequences without any environmental impact. This book is one in a series of books on nuclear power published by InTech. Under the single-volume cover, we put together such topics as operation, safety, environment and radiation effects. The book is not offering a comprehensive coverage of the material in each area. Instead, selected themes are highlighted by authors of individual chapters representing contemporary interests worldwide. With all diversity of topics in 16 chapters, the integrated system analysis approach of nuclear power operation, safety and environment is the common thread. The goal of the book is to bring nuclear power to our readers as one of the promising energy sources that has a unique potential to meet energy demands with minimized environmental impact, near-zero carbon footprint, and competitive economics via robust potential applications. The book targets everyone as its potential readership groups - students, researchers and practitioners - who are interested to learn about nuclear power.

### **How to reference**

In order to correctly reference this scholarly work, feel free to copy and paste the following:

Tomoya Ogawa, Nobuhiko Sarukura, Masahito Watanabe, Tsuguo Fukuda, Nobuhito Nango, Yasunobu Arikawa, Kohei Yamanoi, Tomoharu Nakazato, Marilou Cadatal-Raduban, Toshihiko Shimizu, Mitsuo Nakai, Takayoshi Norimatsu, Hiroshi Azechi, Takahiro Murata, Shigeru Fujino, Hideki Yoshida, Kei Kamada, Yoshiyuki Usuki, Toshihisa Suyama, Akira Yoshikawa, Nakahiro Sato, Hirofumi Kan, Hiroaki Nishimura, Kunioki Mima, Masahito Hosaka, Masahiro Katoh, Nobuhiro Kosugi, Kentaro Fukuda, Takayuki Yanagida, Yuui Yokota, Fumio Saito, Kouhei Sakai, Dirk Ehrentraut, Mitsuru Nagasono, Tadashi Togashi, Atsushi Higashiya, Makina Yabashi, Tetsuya Ishikawa, Haruhiko Ohashi and Hiroaki Kimura (2011). Imaging of Radiation Accidents and Radioactive Contamination Using Scintillators, Nuclear Power - Operation, Safety and Environment, Dr. Pavel Tsvetkov (Ed.), ISBN: 978-953-307-507-5, InTech, Available from: <http://www.intechopen.com/books/nuclear-power-operation-safety-and-environment/imaging-of-radiation-accidents-and-radioactive-contamination-using-scintillators>

**INTECH**  
open science | open minds

[www.intechopen.com](http://www.intechopen.com)

**InTech Europe**

University Campus STeP Ri  
Slavka Krautzeka 83/A  
51000 Rijeka, Croatia  
Phone: +385 (51) 770 447  
Fax: +385 (51) 686 166  
[www.intechopen.com](http://www.intechopen.com)

**InTech China**

Unit 405, Office Block, Hotel Equatorial Shanghai  
No.65, Yan An Road (West), Shanghai, 200040, China  
中国上海市延安西路65号上海国际贵都大饭店办公楼405单元  
Phone: +86-21-62489820  
Fax: +86-21-62489821

IntechOpen

IntechOpen

© 2011 The Author(s). Licensee IntechOpen. This chapter is distributed under the terms of the [Creative Commons Attribution-NonCommercial-ShareAlike-3.0 License](#), which permits use, distribution and reproduction for non-commercial purposes, provided the original is properly cited and derivative works building on this content are distributed under the same license.

IntechOpen

IntechOpen